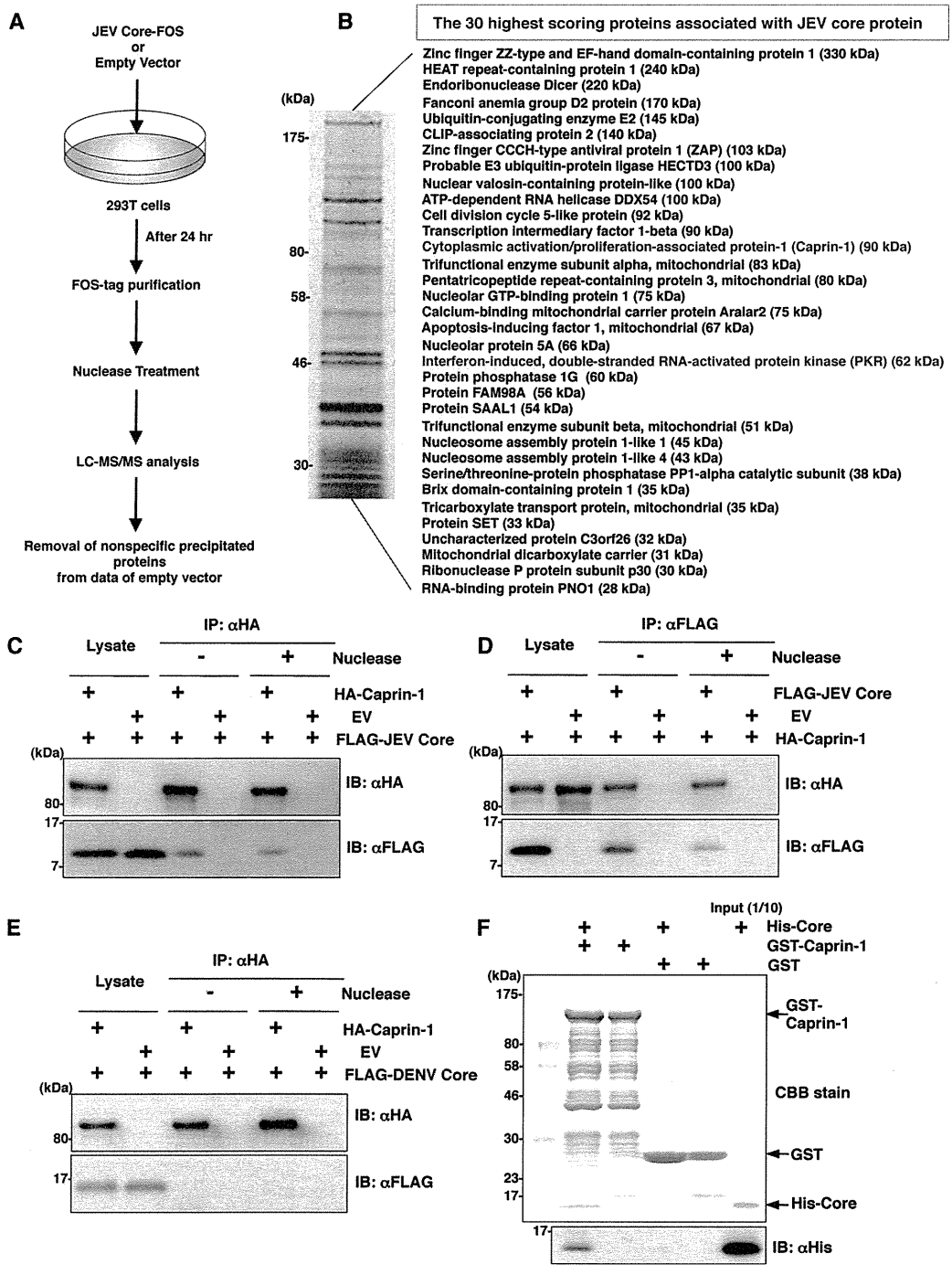

FIG 5 JEV core protein directly interacts with Caprin-1, an SG-associated cellular factor. (A) Identification of host cellular proteins associated with JEV core protein by FOS-tagged purification and LC-MS/MS analysis. Overview of the FOS-tagged purification of cellular proteins associated with JEV core protein. (B) The 30 candidate proteins as binding partners of JEV core protein exhibiting high scores are listed. PKR and Caprin-1 are indicated in red. (C and D) FLAG-JEV core protein and HA-Caprin-1 were coexpressed in 293T cells, and the cell lysates harvested at 24 h posttransfection were treated with or without micrococcal nuclease for 30 min at 37°C and immunoprecipitated (IP) with anti-HA (αHA) or anti-FLAG (αFLAG) antibody, as indicated. The precipitates were subjected to immunoblotting (IB) to detect coprecipitated counterparts. (E) FLAG-DENV core protein was coexpressed with HA-Caprin-1 in 293T cells, immunoprecipitated with anti-HA antibody, and immunoblotted with anti-HA or anti-FLAG antibody. (F) His-tagged JEV core protein was incubated with either GST-fused Caprin-1 or GST for 2 h at 4°C, and the precipitates obtained by GST pulldown assay were subjected to CBB staining and immunoblotting with anti-His antibody.

participate in the inhibition of SG formation, we tried to identify cellular factors associated with the core protein by LC-MS/MS analysis, as shown in Fig. 5A. Among the 30 factors with the best scores, two SG-associated proteins, PKR (Mascot search score, 206) and Caprin-1 (Mascot search score, 153), were identified as binding partners of JEV core protein (Fig. 5B). Although PABP1, hnRNP Q, Staufen, G3BP, and eIF4G were also identified, their scores were lower than those of PKR and Caprin-1. Because the

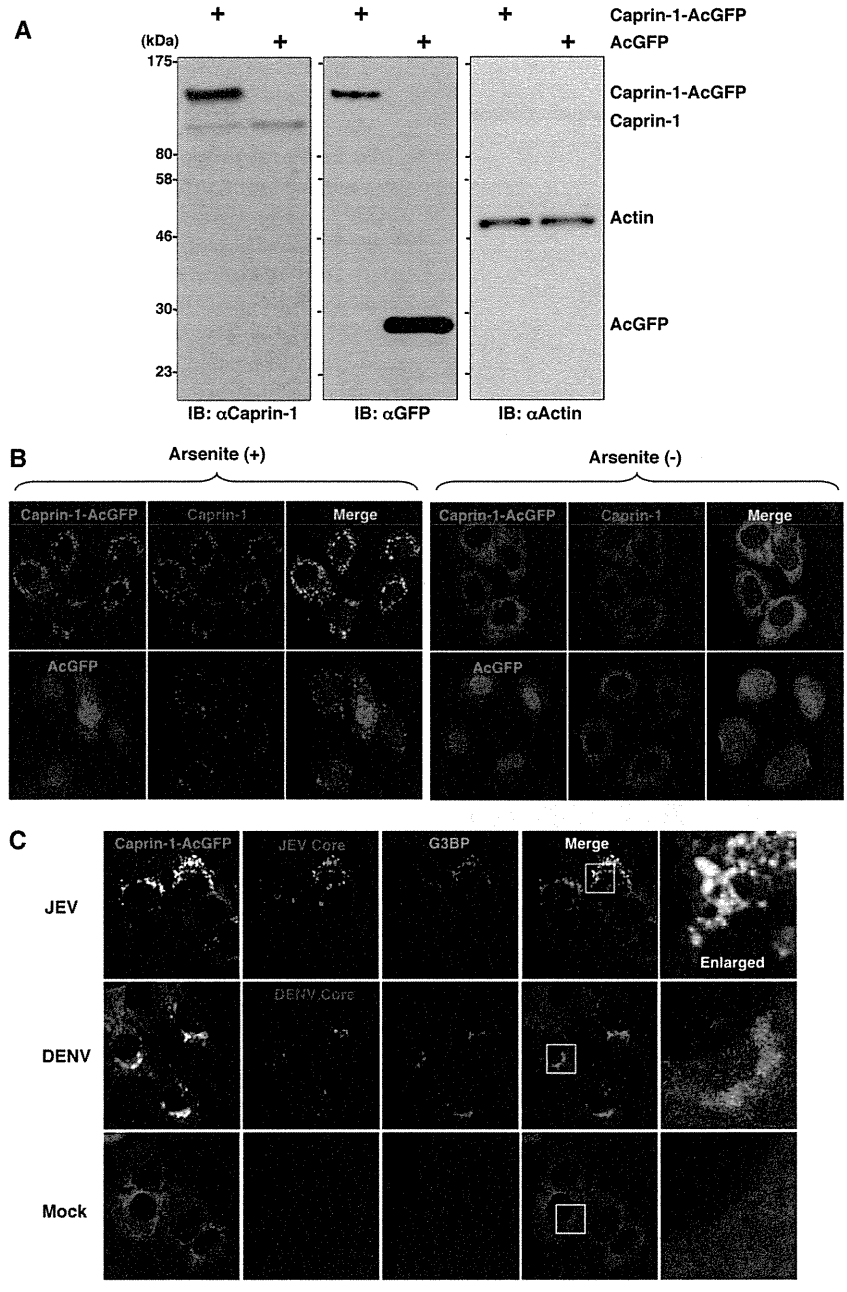

FIG 6 Caprin-1 is colocalized with the JEV core protein in the perinuclear region. (A) Expression of Caprin-1 fused with AcGFP (Caprin-1-AcGFP), Caprin-1, actin, or AcGFP in lentivirally transduced Huh7 cells was determined by immunoblotting using the appropriate antibodies. (B) Subcellular localization of Caprin-1-AcGFP or AcGFP (green) and endogenous Caprin-1 (red) in cells treated with/without 1.0 mM sodium arsenite for 30 min at 37°C was determined by immunofluorescence assay with rabbit anti-Caprin-1 PAb and AF594-conjugated anti-rabbit IgG. Cell nuclei were stained with DAPI (blue). (C) Huh7/Caprin-1-AcGFP cells were infected with either JEV or DENV at an MOI of 0.5, and the cellular localizations of JEV and DENV core (red) with Caprin-1-AcGFP and G3BP (blue) were determined at 24 h and 48 h postinfection, respectively. Cells were stained with mouse anti-G3BP MAb and rabbit anti-JEV or DENV core protein PAb, followed by AF633-conjugated anti-mouse IgG and AF594-conjugated anti-rabbit IgG, respectively, and examined by immunofluorescence analysis.

results shown in Fig. 1B suggest that the inhibition of SG formation takes place downstream of eIF2α phosphorylation, we focused on Caprin-1 as a key factor involved in the inhibition of SG formation in cells infected with JEV. To confirm the specific interaction of JEV core protein with Caprin-1, FLAG-JEV core protein and HA-Caprin-1 were coexpressed and immunoprecipitated with anti-HA or anti-FLAG antibody in the presence or absence of nuclease. FLAG-JEV core protein was coprecipitated with HA-Caprin-1 irrespective of nuclease treatment (Fig. 5C and D), suggesting that the interaction between JEV core protein and Caprin-1 is a protein-protein interaction. On the other hand, FLAG-DENV core protein was not coprecipitated with HA-Caprin-1 (Fig. 5E), indicating that the interaction with Caprin-1 was specific for JEV core protein. Next, the direct interaction be-

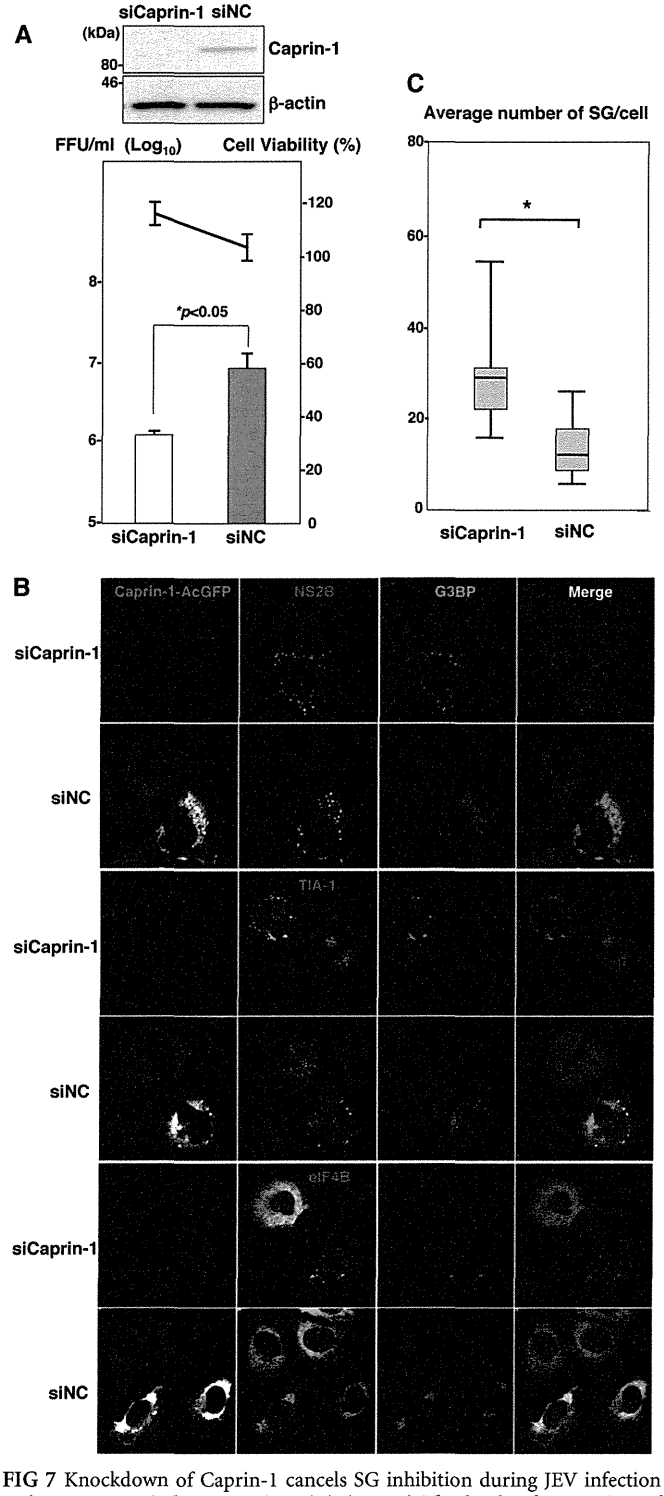

FIG 7 Knockdown of Caprin-1 cancels SG inhibition during JEV infection and suppresses viral propagation. (A) (Upper) The levels of expression of Caprin-1 in cells transfected with either siCaprin-1 or siNC was determined by immunoblotting using anti-Caprin-1 and anti-β-actin antibodies at 72 h posttransfection (top panel). At 48 h posttransfection with either siCaprin-1 or siNC, Huh7/Caprin-1-AcGFP cells were inoculated with JEV at an MOI of 0.5. At 24 h postinfection (72 h posttransfection), the infectious titers in the supernatants were determined by focus-forming assay in Vero cells (bottom panel, bar graph). Cell viability was determined at 72 h posttransfection and calculated as a percentage of the viability of cells treated with siNC (bottom panel, line graph). The results shown are from three independent assays, with the error bars representing the standard deviations. (B) At 48 h posttransfection with either siCaprin-1 or siNC, Huh7/Caprin-1-AcGFP cells were inoculated with JEV at an MOI of 0.5. The cellular localizations of SG-associated factors and JEV NS2B were determined at 24 h postinfection (72 h posttransfection) by immunofluorescence analysis with mouse anti-G3BP MAb and rabbit anti-NS2B PAb, rabbit anti-eIF4B PAb, or goat anti-TIA-1 PAb, followed by AF633-conjugated anti-mouse IgG and AF594-conjugated anti-rabbit IgG or AF594-conjugated anti-goat IgG, respectively. (C) Numbers of G3BP-positive foci in 30 cells prepared as described in panel B were counted. Lines, boxes, and error bars indicate the means, 25th to 75th percentiles, and 95th percentiles, respectively. The significance of differences between the means was determined by a Student's *t* test. *, $P < 0.01$.

tween JEV core protein and Caprin-1 was examined by a GST-pulldown assay using purified proteins expressed in bacteria. The His-tagged core protein was coprecipitated with GST-tagged Caprin-1, suggesting that JEV core protein directly interacts with Caprin-1 (Fig. 5F).

To further determine the cellular localization of Caprin-1 in JEV-infected cells, Caprin-1 fused with AcGFP (Caprin-1-AcGFP) was lentivirally expressed in Huh7 cells. The levels of expression and recruitment of Caprin-1-AcGFP into SGs were determined by immunoblotting and immunofluorescence analysis, respectively (Fig. 6A and B). In cells infected with JEV, Caprin-1-AcGFP was concentrated in the perinuclear region and colocalized with core protein and G3BP, while no colocalization of the proteins was observed in cells infected with DENV (Fig. 6C), suggesting that Caprin-1 directly interacts with JEV core protein in the perinuclear region of the infected cells.

Knockdown of Caprin-1 cancels SG inhibition during JEV infection and suppresses viral propagation. To assess the biological significance of the interaction of JEV core protein with Caprin-1 in JEV propagation, the expression of Caprin-1 was suppressed by using Caprin-1-specific siRNAs (siCaprin-1). Transfection of siCaprin-1 efficiently and specifically knocked down the expression of Caprin-1 with a slight increase of cell viability and decreased the production of infectious particles in the culture supernatants of cells infected with JEV, in comparison with those treated with a control siRNA (siNC) (Fig. 7A). Furthermore, immunofluorescence analyses revealed that knockdown of Caprin-1 increased the number of G3BP-positive granules colocalized with SG-associated factors, including TIA-1 and eIF4B, and inhibited the G3BP concentration in the perinuclear region (Fig. 7B and C). These results suggest that knockdown of Caprin-1 suppresses JEV propagation through the induction of SG formation.

Lys^{97} and Arg^{98} in the JEV core protein are crucial residues for the interaction with Caprin-1. To determine amino acid residues of the core protein that are required for the interaction with Caprin-1, we constructed a putative model based on the structural information of the DENV core protein previously resolved by nuclear magnetic resonance (NMR) (27), as shown in Fig. 8A. Based on this model, we selected hydrophobic amino acids, which were located on the solvent-exposed side in the α1 and α4 helices, as amino acid residues responsible for the binding to host proteins. Amino acid substitutions in each of the α-helices shown in Fig. 8B were designed in the context of FLAG-Core (Mα1 and Mα4), and the interaction of FLAG-Core mutants with Caprin-1 was examined by immunoprecipitation analysis. WT and Mα1, but not Mα4, core proteins were immunoprecipitated with Caprin-1 (Fig. 8B). To determine the amino acids responsible for interaction with Caprin-1, further alanine substitutions were introduced in the α4 helix, and the interaction was examined by immunopre-

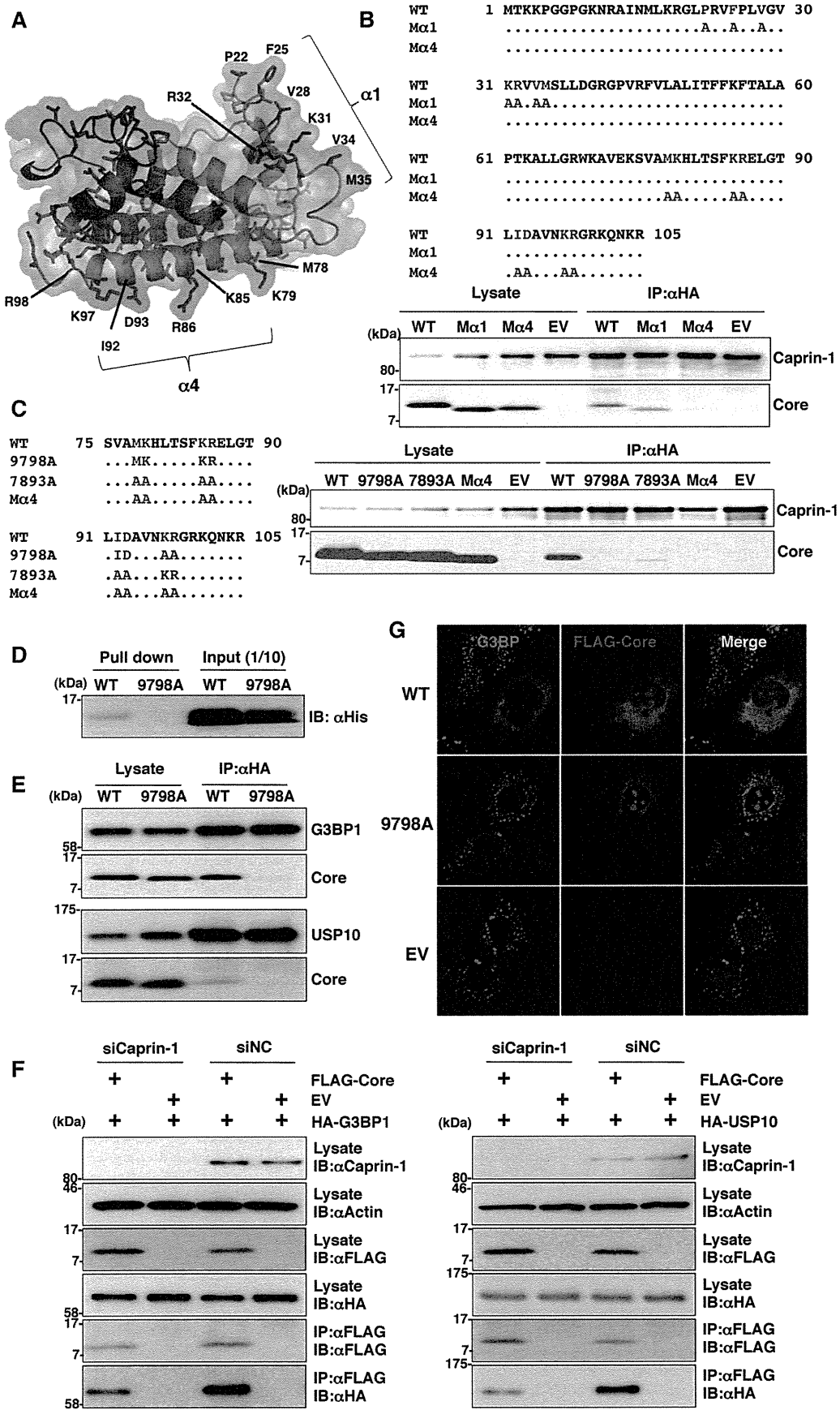

cipitation assay. As shown in Fig. 8C, double replacing both Lys^{97} and Arg^{98} with Ala (9798A) completely abrogated the interaction with Caprin-1. The importance of these two amino acids in the interaction with Caprin-1 was also confirmed by GST pulldown assay (Fig. 8D). These results indicate that Lys^{97} and Arg^{98} in the JEV core protein are crucial for the interaction with Caprin-1. Since G3BP has been reported to be one of the key molecules for SG formation and interacts with several SG component molecules including Caprin-1 and USP10 (28, 29), interactions of the core protein with SG components were examined by immunoprecipitation assay. The wild-type but not mutant 9798A core protein was associated with G3BP1 and USP10 (Fig. 8E). In addition, the knockdown of Caprin-1 weakened the interactions of core protein with G3BP1 or USP10 (Fig. 8F). These findings indicate that JEV core protein associates with several SG component molecules, such as G3BP1 and USP10, through the interaction with Caprin-1. Next, the role of the interaction between JEV core protein and Caprin-1 in the suppression of SG formation was examined by immunofluorescence analysis. Although the expression of the wild-type JEV core protein suppressed the SG formation induced by sodium arsenite treatment, as shown above, expression of the 9798A mutant did not (Fig. 8G), suggesting that the interaction of JEV core protein with Caprin-1 through Lys^{97} and Arg^{98} plays a crucial role in the inhibition of SG formation.

Interaction of the JEV core protein with Caprin-1 plays crucial roles not only in viral propagation *in vitro* but also in the pathogenesis in mice through the suppression of SG formation. To further examine the biological significance of the interaction between the JEV core protein and Caprin-1 in viral replication, we generated a mutant infectious cDNA clone (pMWJEAT/9798AA) of JEV encoding a mutant core protein deficient in the binding to Caprin-1 based on pMWJEAT. First, the cellular localization of the core protein in the 9798A mutant JEV-infected cells was examined by immunofluorescence analysis. The 9798A mutant core protein, as well as the wild-type core protein, was localized in the nucleus and the perinuclear region (Fig. 9A). However, the 9798A mutant core protein was not colocalized with Caprin-1, in contrast to the wild-type core protein. The sizes of infectious foci in Vero cells infected with the 9798A mutant were significantly smaller than those infected with the wild-type JEV (Fig. 9B). Furthermore, the infectious titers in C6/36 and Vero cells infected with the 9798A mutant were 6.1- and 12.6-fold lower than those infected with wild-type JEV at 48 h postinfection, respectively (Fig. 9C), suggesting that interaction of the JEV core protein with Caprin-1 plays crucial roles in the propagation of JEV in both insect and mammalian cells. Cells infected with the 9798A mutant induced SGs containing both G3BP and Caprin-1, in contrast to the accumulation of G3BP in the perinuclear region observed in those infected with the wild-type JEV (Fig. 9D). The numbers of foci in cells infected with the 9798A mutant were higher than those in cells infected with the wild-type JEV (Fig. 9E), indicating that the interaction of the JEV core protein with Caprin-1 is crucial for the suppression of SG formation. Finally, we examined the biological relevance of the interaction of JEV core protein with Caprin-1 in viral replication *in vivo*. Infectious particles were recovered from the cerebrums of ICR mice inoculated with wild-type JEV but not from those inoculated with the 9798A mutant (Fig. 9F). In addition, all 10 mice had died by 12 days postinoculation with the wild-type JEV, while only 1 mouse had died at day 10 postinoculation with the 9798A mutant (Fig. 9G). Collectively, these results suggest that the interaction of JEV core protein with Caprin-1 plays crucial roles not only in viral replication *in vitro* but also in pathogenesis in mice through the suppression of SG formation.

DISCUSSION

Viruses are obligatory intracellular parasites, and their life cycles rely on host cellular functions. Many viruses have evolved to inhibit SG formation and thereby evade the host translation shutoff mechanism and facilitate viral replication (6, 30), while some viruses co-opt molecules regulating SG formation for viral replication (11, 31). The vaccinia virus subverts SG components to generate aggregates containing G3BP, Caprin-1, eIF4G, eIF4E, and mRNA of the virus, but not of the host, in order to stimulate viral translation (11). Replication, translation, and assembly of transmissible gastroenteritis coronavirus, a member of the *Coronaviridae* family, are regulated by the interaction of polypyrimidine tract-binding protein and TIA-1 with viral RNA (31). HIV-1 utilizes Staufen1, which is a principal component of SG, in the viral RNA selection to form ribonucleoproteins (RNPs) through interaction with Gag protein, instead of SG translation silencing (8). In the case of flaviviruses, TIA-1 and TIAR bind to the 3′ untranslated region (UTR) of the negative-stranded RNA of WNV to facilitate viral replication (16), and G3BP1, Caprin-1, and USP10 interact with DENV RNA, although the biological significance of these interactions remains unknown (26). In this study, we have shown that JEV infection suppresses SG formation by the recruitment of several effector molecules promoting SG assembly, including G3BP and USP10, to the perinuclear region through the interaction of JEV core protein with Caprin-1. Furthermore, a mutant JEV carrying a core protein incapable of binding to

FIG 8 Lys^{97} and Arg^{98} in the JEV core protein are crucial residues for the interaction with Caprin-1. (A) Putative structural model of the core protein homodimer of JEV deduced from that of DENV obtained from the Protein Data Bank (accession number 1R6R) by using PyMOL software. The two α helices (α1 and α4) are indicated. (B) FLAG-Core mutants in which the hydrophobic amino acid residues in the α1 helix (Mα1) or α4 helix (Mα4) were replaced with alanine were coexpressed with HA-Caprin-1 in 293T cells, immunoprecipitated (IP) with anti-HA antibody, and examined by immunoblotting (IB) with anti-HA or anti-FLAG antibody. (C) FLAG-Core mutants in which the Met^{78}, Lys^{79}, Lys^{85}, Arg^{86}, Ile^{92}, and Asp^{93} (7893A) or Lys^{97} and Arg^{98} (9798A) in the α4 helix domain were replaced with alanine were coexpressed with HA-Caprin-1 in 293T cells and examined as described in panel B. (D) The His-tagged JEV core protein (WT or 9798A) was incubated with GST-fused Caprin-1 for 2 h at 4°C, and the precipitates obtained by GST pulldown assay were subjected to immunoblotting with anti-His antibody. (E) FLAG-Core (WT or 9798A) was coexpressed with HA-G3BP1 or HA-USP10 in 293T cells, immunoprecipitated with anti-HA antibody, and immunoblotted with anti-HA and anti-FLAG antibodies. (F) FLAG-JEV Core was coexpressed with HA-G3BP1 or HA-USP10 in 293T cells transfected with either siCaprin-1 or siNC at 72 h posttransfection, immunoprecipitated with anti-FLAG antibody, and immunoblotted with anti-HA and anti-FLAG antibodies. The cell lysates were also subjected to immunoblotting with anti-Caprin-1 and anti-β-actin antibodies to evaluate the knockdown efficiency of Caprin-1. (G) The cellular localizations of G3BP and FLAG-Core (WT or 9798A) were determined at 24 h posttransfection after treatment with 1.0 mM sodium arsenite for 30 min at 37°C by immunofluorescence analysis with mouse anti-G3BP MAb and rabbit anti-FLAG PAb, followed by AF488-conjugated anti-mouse IgG and AF594-conjugated anti-rabbit IgG, respectively. Cell nuclei were stained with DAPI (blue).

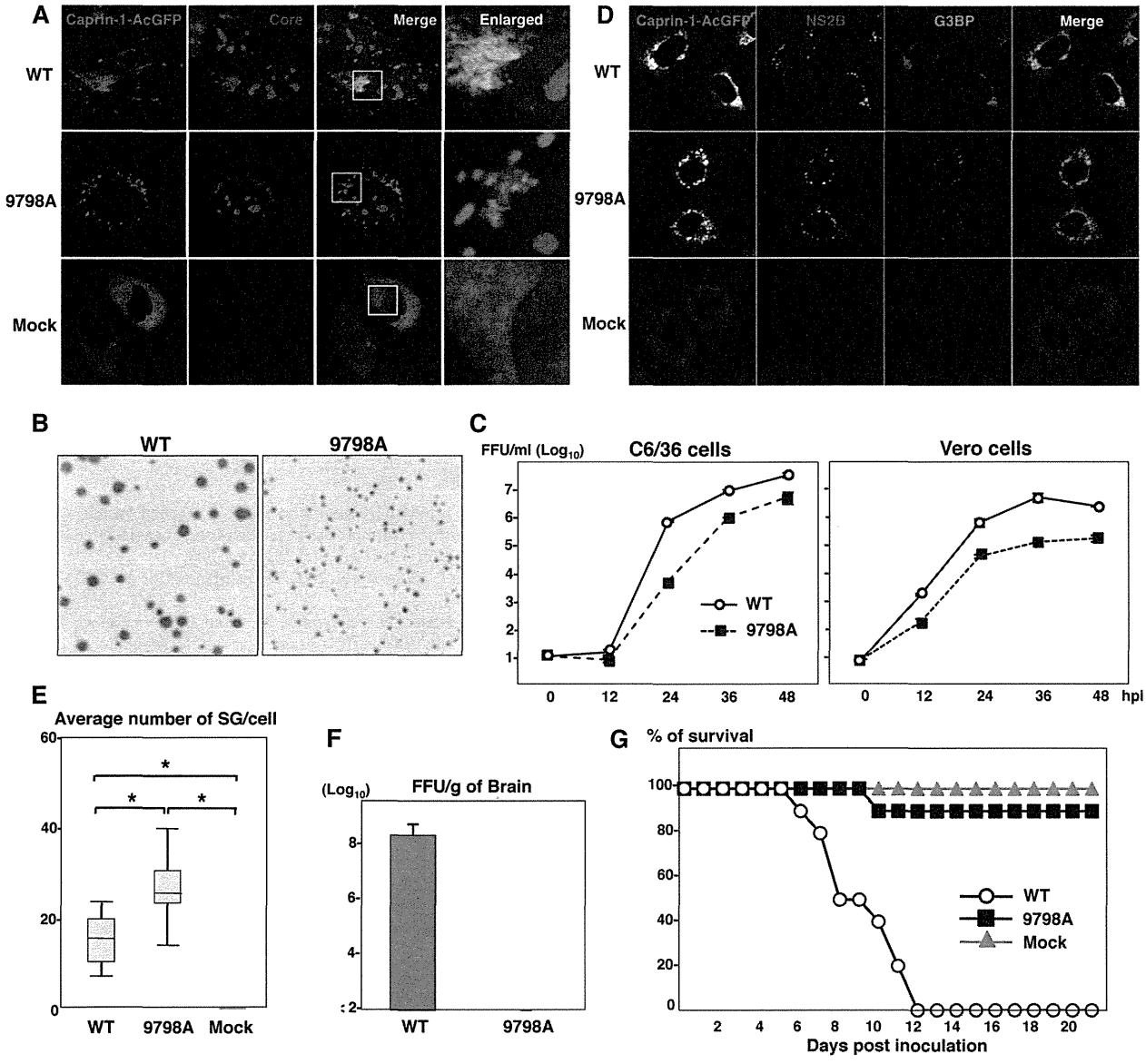

FIG 9 Interaction of JEV core protein with Caprin-1 plays crucial roles not only in viral replication *in vitro* but also in pathogenesis in mice through the suppression of SG formation. (A) Huh7/Caprin-1-AcGFP cells were infected with JEV (WT or 9798A mutant) at an MOI of 1.0, and the cellular localizations of Caprin-1-AcGFP and JEV core protein were determined at 24 h postinfection by immunofluorescence analysis with rabbit anti-core PAb and AF594-conjugated anti-rabbit IgG. Cell nuclei were stained with DAPI (blue). (B) Focus formation of JEV (WT or 9798A mutant) in Vero cells incubated in methylcellulose overlay medium at 48 h postinfection. The infectious foci were immunostained as described previously (20). (C) Growth kinetics of JEV (WT or 9798A mutant) in C6/36 and Vero cells infected at an MOI of 0.1. Infectious titers in the culture supernatants harvested at the indicated times were determined by focus-forming assays in Vero cells. Means of three experiments are indicated. (D) Huh7/Caprin-1-AcGFP cells were infected with either WT or 9798A at an MOI of 0.5, and cellular localizations of Caprin-1-AcGFP, G3BP (blue), and JEV NS2B (red) were determined at 24 h postinfection by immunofluorescence analysis with mouse anti-G3BP MAb and rabbit anti-NS2B PAb, followed by AF633-conjugated anti-mouse IgG and AF594-conjugated anti-rabbit IgG, respectively. (E) Numbers >of G3BP-positive foci in 30 cells prepared as described in panel D were counted. Lines, boxes, and error bars indicate the means, 25th to 75th percentiles, and 95th percentiles, respectively. The significance of differences between the means was determined by Student's *t* test. *, $P < 0.01$. (F) Infectious titers in the cerebrums of mice at 7 days postintraperitoneal inoculation with 5×10^4 FFU/100 μl of either WT or 9798A virus were determined in Vero cells. The means of titers in the homogenates of the cerebrums from three mice are indicated. The detection limit is 10^2 FFU/g of cerebrum. (G) Percentages of surviving mice ($n = 10$) after intraperitoneal inoculation with 5×10^4 FFU of either WT or 9798A virus. Mock, inoculation with DMEM.

Caprin-1 exhibited reduced replication *in vitro* and attenuated pathogenicity in mice.

G3BP is one of the key molecules involved in the SG aggregation process and self-oligomerizes in a phosphorylation-dependent manner to sequester mRNA in SGs (4). Therefore, G3BP knocked down cells (6) and G3BP knockout mouse embryonic fibroblast cells are deficient in the SG formation. In addition, G3BP sequestration inhibits SG formation in response to arsenite treatment (32). Caprin-1, known as RNA granule protein 105 or p137 (33), also participates in SG formation through phosphorylation of eIF2α (28) and is ubiquitously expressed in the cytoplasm. Caprin-1 regulates the transport and translation of mRNAs

of proteins involved in the synaptic plasticity in neurons (34) and cellular proliferation and migration in multiple cell types (28) through an interaction with G3BP. USP10, another SG-associated molecule, also interacts with G3BP and forms the G3BP/USP10 complex (29), suggesting that several SG-associated RBPs participate in the formation of a protein-protein network. In this study, the JEV core protein was shown to directly interact with Caprin-1, to sequester several key molecule complexes involved in SG formation to the perinuclear region in cells infected with JEV, and to facilitate viral propagation through the suppression of SG formation.

Flaviviruses replicate at a relatively low rate in comparison with most of the other positive-stranded RNA viruses, and thus rapid shutdown of host cellular protein synthesis would be deleterious for the viral life cycle. In cells infected with JEV, several SG components were colocalized with the core protein in the perinuclear region, while in those infected with WNV or DENV, SG components were accumulated in a replication complex composed of viral RNA and nonstructural proteins. In addition, the phosphorylation of eIF2α induced by arsenite was completely canceled by the infection with WNV or DENV, whereas the suppression of the phosphorylation was limited in JEV infection (15). Incorporation of the nascent viral RNA into the membranous structure induced by viral nonstructural proteins prevents PKR activation and inhibits SG formation in cells infected with WNV (17). In cells infected with hepatitis C virus (HCV), which belongs to the genus *Hepacivirus* in the family *Flaviviridae*, induction of SG formation was observed in the early stage of infection, in contrast to the inhibition of the arsenite-induced SG formation in the late stage (35). Several SG components, such as G3BP1, PABP1, and ataxin-2, were colocalized with HCV core protein around lipid droplets (35), and G3BP1 was also associated with the NS5B protein and the 5′ terminus of the minus-strand viral RNA (36) to mediate efficient viral replication. Collectively, these data suggest that flaviviruses have evolved to regulate cellular processes involved in SG formation through various strategies.

PKR is one of the interferon-stimulated genes and plays a crucial role in antiviral defense through phosphorylation of eIF2α, which leads to host translational shutoff (37, 38). In the early stage of flavivirus infection, both positive- and negative-stranded RNAs transcribe at low levels, while genomic RNA predominantly synthesizes in the late stage of infection (39). It was shown that activation of PKR was suppressed (40) or only induced in the late stage of WNV infection (41) and impaired by the expression of HCV NS5A (42–44). Very recently, JEV NS2A was shown to suppress PKR activation through inhibition of dimerization of PKR in the early stage but not in the late stage of infection (45). In this study, we have shown that JEV core protein interacts with Caprin-1 and inhibits SG formation downstream of the phosphorylation of eIF2α in the late stage of infection, suggesting that JEV has evolved to escape from host antiviral responses in the multiple stages of viral replication by using structural and nonstructural proteins.

The flavivirus core protein is a multifunctional protein involved in many aspects of the viral life cycle. In addition to the formation of viral nucleocapsid through the interaction with viral RNA (as a structural protein) (46), flavivirus core proteins interact with various host factors, such as B23 (47), Jab1 (48), hnRNP K (49), and hnRNP A2 (23), and regulate viral replication and/or modify the host cell environment (as a nonstructural protein). Although further investigations are needed to clarify the precise mechanisms underlying the circumvention of SG formation through the interaction of JEV core protein with Caprin-1, leading to efficient propagation *in vitro* and pathogenicity in mice, these findings could help not only to provide new insight into strategies by which viruses escape host stress responses but also to develop novel antiviral agents for flavivirus infection.

ACKNOWLEDGMENTS

We thank M. Tomiyama for secretarial assistance. We also thank K. Saito and T. Wakita for technical advice and the infectious clone of JEV, respectively.

This work was supported in part by grants-in-aid from the Ministry of Health, Labor, and Welfare, the Ministry of Education, Culture, Sports, Science, and Technology, and the Osaka University Global Center of Excellence Program. H. Katoh is a research fellow of the Japanese Society for the Promotion of Science.

REFERENCES

1. **Nover L, Scharf KD, Neumann D.** 1989. Cytoplasmic heat shock granules are formed from precursor particles and are associated with a specific set of mRNAs. Mol. Cell. Biol. **9**:1298–1308.
2. **Anderson P, Kedersha N.** 2002. Stressful initiations. J. Cell Sci. **115**:3227–3234.
3. **Gilks N, Kedersha N, Ayodele M, Shen L, Stoecklin G, Dember LM, Anderson P.** 2004. Stress granule assembly is mediated by prion-like aggregation of TIA-1. Mol. Biol. Cell **15**:5383–5398.
4. **Tourriere H, Chebli K, Zekri L, Courselaud B, Blanchard JM, Bertrand E, Tazi J.** 2003. The RasGAP-associated endoribonuclease G3BP assembles stress granules. J. Cell Biol. **160**:823–831.
5. **Kedersha N, Cho MR, Li W, Yacono PW, Chen S, Gilks N, Golan DE, Anderson P.** 2000. Dynamic shuttling of TIA-1 accompanies the recruitment of mRNA to mammalian stress granules. J. Cell Biol. **151**:1257–1268.
6. **White JP, Cardenas AM, Marissen WE, Lloyd RE.** 2007. Inhibition of cytoplasmic mRNA stress granule formation by a viral proteinase. Cell Host Microbe **2**:295–305.
7. **Khaperskyy DA, Hatchette TF, McCormick C.** 2012. Influenza A virus inhibits cytoplasmic stress granule formation. FASEB J. **26**:1629–1639.
8. **Abrahamyan LG, Chatel-Chaix L, Ajamian L, Milev MP, Monette A, Clement JF, Song R, Lehmann M, DesGroseillers L, Laughrea M, Boccaccio G, Mouland AJ.** 2010. Novel Staufen1 ribonucleoproteins prevent formation of stress granules but favour encapsidation of HIV-1 genomic RNA. J. Cell Sci. **123**:369–383.
9. **McInerney GM, Kedersha NL, Kaufman RJ, Anderson P, Liljestrom P.** 2005. Importance of eIF2α phosphorylation and stress granule assembly in alphavirus translation regulation. Mol. Biol. Cell **16**:3753–3763.
10. **Smith JA, Schmechel SC, Raghavan A, Abelson M, Reilly C, Katze MG, Kaufman RJ, Bohjanen PR, Schiff LA.** 2006. Reovirus induces and benefits from an integrated cellular stress response. J. Virol. **80**:2019–2033.
11. **Katsafanas GC, Moss B.** 2007. Colocalization of transcription and translation within cytoplasmic poxvirus factories coordinates viral expression and subjugates host functions. Cell Host Microbe **2**:221–228.
12. **Misra UK, Kalita J.** 2010. Overview: Japanese encephalitis. Prog. Neurobiol. **91**:108–120.
13. **Sumiyoshi H, Mori C, Fuke I, Morita K, Kuhara S, Kondou J, Kikuchi Y, Nagamatu H, Igarashi A.** 1987. Complete nucleotide sequence of the Japanese encephalitis virus genome RNA. Virology **161**:497–510.
14. **Murray CL, Jones CT, Rice CM.** 2008. Architects of assembly: roles of *Flaviviridae* non-structural proteins in virion morphogenesis. Nat. Rev. Microbiol. **6**:699–708.
15. **Emara MM, Brinton MA.** 2007. Interaction of TIA-1/TIAR with West Nile and dengue virus products in infected cells interferes with stress granule formation and processing body assembly. Proc. Natl. Acad. Sci. U. S. A. **104**:9041–9046.
16. **Li W, Li Y, Kedersha N, Anderson P, Emara M, Swiderek KM, Moreno GT, Brinton MA.** 2002. Cell proteins TIA-1 and TIAR interact with the 3′ stem-loop of the West Nile virus complementary minus-strand RNA and facilitate virus replication. J. Virol. **76**:11989–12000.
17. **Courtney SC, Scherbik SV, Stockman BM, Brinton MA.** 2012. West Nile

virus infections suppress early viral RNA synthesis and avoid inducing the cell stress granule response. J. Virol. 86:3647–3657.
18. Kambara H, Tani H, Mori Y, Abe T, Katoh H, Fukuhara T, Taguwa S, Moriishi K, Matsuura Y. 2011. Involvement of cyclophilin B in the replication of Japanese encephalitis virus. Virology 412:211–219.
19. Mori Y, Yamashita T, Tanaka Y, Tsuda Y, Abe T, Moriishi K, Matsuura Y. 2007. Processing of capsid protein by cathepsin L plays a crucial role in replication of Japanese encephalitis virus in neural and macrophage cells. J. Virol. 81:8477–8487.
20. Mori Y, Okabayashi T, Yamashita T, Zhao Z, Wakita T, Yasui K, Hasebe F, Tadano M, Konishi E, Moriishi K, Matsuura Y. 2005. Nuclear localization of Japanese encephalitis virus core protein enhances viral replication. J. Virol. 79:3448–3458.
21. Kambara H, Fukuhara T, Shiokawa M, Ono C, Ohara Y, Kamitani W, Matsuura Y. 2012. Establishment of a novel permissive cell line for the propagation of hepatitis C virus by expression of microRNA miR122. J. Virol. 86:1382–1393.
22. Zhao Z, Date T, Li Y, Kato T, Miyamoto M, Yasui K, Wakita T. 2005. Characterization of the E-138 (Glu/Lys) mutation in Japanese encephalitis virus by using a stable, full-length, infectious cDNA clone. J. Gen. Virol. 86:2209–2220.
23. Katoh H, Mori Y, Kambara H, Abe T, Fukuhara T, Morita E, Moriishi K, Kamitani W, Matsuura Y. 2011. Heterogeneous nuclear ribonucleoprotein A2 participates in the replication of Japanese encephalitis virus through an interaction with viral proteins and RNA. J. Virol. 85:10976–10988.
24. Hamamoto I, Nishimura Y, Okamoto T, Aizaki H, Liu M, Mori Y, Abe T, Suzuki T, Lai MM, Miyamura T, Moriishi K, Matsuura Y. 2005. Human VAP-B is involved in hepatitis C virus replication through interaction with NS5A and NS5B. J. Virol. 79:13473–13482.
25. Jones CT, Ma L, Burgner JW, Groesch TD, Post CB, Kuhn RJ. 2003. Flavivirus capsid is a dimeric alpha-helical protein. J. Virol. 77:7143–7149.
26. Ward AM, Bidet K, Yinglin A, Ler SG, Hogue K, Blackstock W, Gunaratne J, Garcia-Blanco MA. 2011. Quantitative mass spectrometry of DENV-2 RNA-interacting proteins reveals that the DEAD-box RNA helicase DDX6 binds the DB1 and DB2 3′ UTR structures. RNA Biol. 8:1173–1186.
27. Ma L, Jones CT, Groesch TD, Kuhn RJ, Post CB. 2004. Solution structure of dengue virus capsid protein reveals another fold. Proc. Natl. Acad. Sci. U. S. A. 101:3414–3419.
28. Solomon S, Xu Y, Wang B, David MD, Schubert P, Kennedy D, Schrader JW. 2007. Distinct structural features of Caprin-1 mediate its interaction with G3BP-1 and its induction of phosphorylation of eukaryotic translation initiation factor 2α, entry to cytoplasmic stress granules, and selective interaction with a subset of mRNAs. Mol. Cell. Biol. 27:2324–2342.
29. Soncini C, Berdo I, Draetta G. 2001. Ras-GAP SH3 domain binding protein (G3BP) is a modulator of USP10, a novel human ubiquitin specific protease. Oncogene 20:3869–3879.
30. Montero H, Rojas M, Arias CF, Lopez S. 2008. Rotavirus infection induces the phosphorylation of eIF2α but prevents the formation of stress granules. J. Virol. 82:1496–1504.
31. Sola I, Galan C, Mateos-Gomez PA, Palacio L, Zuniga S, Cruz JL, Almazan F, Enjuanes L. 2011. The polypyrimidine tract-binding protein affects coronavirus RNA accumulation levels and relocalizes viral RNAs to novel cytoplasmic domains different from replication-transcription sites. J. Virol. 85:5136–5149.
32. Hinton SD, Myers MP, Roggero VR, Allison LA, Tonks NK. 2010. The pseudophosphatase MK-STYX interacts with G3BP and decreases stress granule formation. Biochem. J. 427:349–357.
33. Grill B, Wilson GM, Zhang KX, Wang B, Doyonnas R, Quadroni M, Schrader JW. 2004. Activation/division of lymphocytes results in increased levels of cytoplasmic activation/proliferation-associated protein-1: prototype of a new family of proteins. J. Immunol. 172:2389–2400.
34. Shiina N, Shinkura K, Tokunaga M. 2005. A novel RNA-binding protein in neuronal RNA granules: regulatory machinery for local translation. J. Neurosci. 25:4420–4434.
35. Ariumi Y, Kuroki M, Kushima Y, Osugi K, Hijikata M, Maki M, Ikeda M, Kato N. 2011. Hepatitis C virus hijacks P-body and stress granule components around lipid droplets. J. Virol. 85:6882–6892.
36. Yi Z, Pan T, Wu X, Song W, Wang S, Xu Y, Rice CM, Macdonald MR, Yuan Z. 2011. Hepatitis C virus co-opts Ras-GTPase-activating protein-binding protein 1 for its genome replication. J. Virol. 85:6996–7004.
37. Gale M, Jr, Katze MG. 1998. Molecular mechanisms of interferon resistance mediated by viral-directed inhibition of PKR, the interferon-induced protein kinase. Pharmacol. Ther. 78:29–46.
38. Pindel A, Sadler A. 2011. The role of protein kinase R in the interferon response. J. Interferon Cytokine Res. 31:59–70.
39. Chu PW, Westaway EG. 1985. Replication strategy of Kunjin virus: evidence for recycling role of replicative form RNA as template in semiconservative and asymmetric replication. Virology 140:68–79.
40. Elbahesh H, Scherbik SV, Brinton MA. 2011. West Nile virus infection does not induce PKR activation in rodent cells. Virology 421:51–60.
41. Samuel MA, Whitby K, Keller BC, Marri A, Barchet W, Williams BR, Silverman RH, Gale M, Jr, Diamond MS. 2006. PKR and RNase L contribute to protection against lethal West Nile Virus infection by controlling early viral spread in the periphery and replication in neurons. J. Virol. 80:7009–7019.
42. Gale M, Jr, Blakely CM, Kwieciszewski B, Tan SL, Dossett M, Tang NM, Korth MJ, Polyak SJ, Gretch DR, Katze MG. 1998. Control of PKR protein kinase by hepatitis C virus nonstructural 5A protein: molecular mechanisms of kinase regulation. Mol. Cell. Biol. 18:5208–5218.
43. Gale MJ, Jr, Korth MJ, Tang NM, Tan SL, Hopkins DA, Dever TE, Polyak SJ, Gretch DR, Katze MG. 1997. Evidence that hepatitis C virus resistance to interferon is mediated through repression of the PKR protein kinase by the nonstructural 5A protein. Virology 230:217–227.
44. He Y, Tan SL, Tareen SU, Vijaysri S, Langland JO, Jacobs BL, Katze MG. 2001. Regulation of mRNA translation and cellular signaling by hepatitis C virus nonstructural protein NS5A. J. Virol. 75:5090–5098.
45. Tu YC, Yu CY, Liang JJ, Lin E, Liao CL, Lin YL. 2012. Blocking dsRNA-activated protein kinase PKR by Japanese encephalitis virus nonstructural protein 2A. J. Virol. 86:10347–10358.
46. Khromykh AA, Westaway EG. 1996. RNA binding properties of core protein of the flavivirus Kunjin. Arch. Virol. 141:685–699.
47. Tsuda Y, Mori Y, Abe T, Yamashita T, Okamoto T, Ichimura T, Moriishi K, Matsuura Y. 2006. Nucleolar protein B23 interacts with Japanese encephalitis virus core protein and participates in viral replication. Microbiol. Immunol. 50:225–234.
48. Oh W, Yang MR, Lee EW, Park KM, Pyo S, Yang JS, Lee HW, Song J. 2006. Jab1 mediates cytoplasmic localization and degradation of West Nile virus capsid protein. J. Biol. Chem. 281:30166–30174.
49. Chang CJ, Luh HW, Wang SH, Lin HJ, Lee SC, Hu ST. 2001. The heterogeneous nuclear ribonucleoprotein K (hnRNP K) interacts with dengue virus core protein. DNA Cell Biol. 20:569–577.

Citation: Cell Death and Disease (2012) 3, e404; doi:10.1038/cddis.2012.130

www.nature.com/cddis

Bcl-2 family member Bcl-G is not a proapoptotic protein

M Giam[1,2], T Okamoto[1,2,3], JD Mintern[1,2,4], A Strasser[1,2] and P Bouillet[1,2]

The three major subgroups of the Bcl-2 family, including the prosurvival Bcl-2-like proteins, the proapoptotic Bcl-2 homology (BH)3-only proteins and Bax/Bak proteins, regulate the mitochondrial apoptotic pathway. In addition, some outliers within the Bcl-2 family do not fit into these subgroups. One of them, Bcl-G, has a BH2 and a BH3 region, and was proposed to trigger apoptosis. To investigate the physiological role of Bcl-G, we have inactivated the gene in the mouse and generated monoclonal antibodies to determine its expression. Although two isoforms of Bcl-G exist in human, only one is found in mice. mBcl-G is expressed in a range of epithelial as well as in dendritic cells. Loss of Bcl-G did not appear to affect any of these cell types. mBcl-G only binds weakly to prosurvival members of the Bcl-2 family, and in a manner that is independent of its BH3 domain. To understand what the physiological role of Bcl-G might be, we searched for Bcl-G-binding partners through immunoprecipitation/mass spectroscopy and yeast-two-hybrid screening. Although we did not uncover any Bcl-2 family member in these screens, we found that Bcl-G interacts specifically with proteins of the transport particle protein complex. We conclude that Bcl-G most probably does not function in the classical stress-induced apoptosis pathway, but rather has a role in protein trafficking inside the cell.

Cell Death and Disease (2012) **3,** e404; doi:10.1038/cddis.2012.130; published online 11 October 2012
Subject Category: Cancer

Proteins of the Bcl-2 family are divided into three subgroups according to their function and the presence of characteristic Bcl-2 homology (BH) domains. The prosurvival members (Bcl-2, Bcl-x_L, Bcl-w, Mcl-1 and A1/Bfl-1) contain four BH domains and are critical for cell survival. The proapoptotic proteins Bax and Bak, which also contain all four BH domains and are structurally similar to their prosurvival relatives, are essential for mitochondrial outer membrane permeabilisation. The BH3-only proteins (Bim, Bid, Puma, Bmf, Bik, Bad, Noxa and Hrk) are essential initiators of apoptosis that cause activation of Bax and Bak, either directly or indirectly by binding to and blocking the prosurvival Bcl-2 family members.[1] The presence of the BH1, BH2 and BH3 domains in the multi-domain proteins determines their three-dimensional structure, in particular the existence on their surface of a groove that functions as a receptor for the BH3 domain of BH3-only or the Bax/Bak proteins. Mutations in the conserved residues of the BH3 domain of proapoptotic proteins almost invariably modify or abrogate their interaction with the groove of the prosurvival Bcl-2-like proteins.[2]

A number of other proteins harbouring a BH3-like domain (and sometimes another BH domain) have been described.[3] Although many of these proteins have been included in the Bcl-2 family, their role in stress-induced apoptosis is often controversial, and some of these proteins have even been implicated in diverse non-apoptotic cellular functions, such as cell cycle regulation, DNA repair, ubiquitination, metabolism or autophagy.[3]

BCL-G, also known as BCL2L14, was first described as a novel proapoptotic member of the Bcl-2 family.[4] The human *BCL-G* gene encodes two major isoforms, BCL-G_L and BCL-G_S. BCL-G_L contains both BH3 and BH2 domains, whereas BCL-G_S contains only the BH3 domain. BCL-G_S was reported to kill cells by binding and neutralisation of prosurvival BCL-X_L. In contrast, BCL-G_L did not bind BCL-X_L and showed only poor killing activity.[4] Mouse Bcl-G is 68% identical and 78% similar to human BCL-G_L.[5] Functional characterisation of mBcl-G has been limited, and most studies have considered its proapoptotic nature as a fait accompli.

To characterise this unusual member of the Bcl-2 family, we have generated highly specific monoclonal antibodies (mAb) and Bcl-G-deficient mice. Our results highlight differences between the mouse and human *Bcl-G* genes and suggest that Bcl-G may not function as a classical BH3-only protein.

[1]The Walter and Eliza Hall Institute of Medical Research, Melbourne, VIC, Australia and [2]Department of Medical Biology, University of Melbourne, Melbourne, VIC, Australia
*Corresponding author: P Bouillet, The Walter and Eliza Hall Institute of Medical Research, Molecular Genetics of Cancer Division, 1G Royal Parade, Parkville, VIC 3052, Australia. Tel: +61 3 9345 2334; Fax: +61 3 9347 0852; E-mail: bouillet@wehi.edu.au
[3]Current address: Department of Molecular Virology, Research Institute for Microbial Diseases, Osaka University, Osaka, Japan.
[4]Current address: Department of Biochemistry and Molecular Biology, University of Melbourne, Melbourne, VIC, Australia.
Keywords: apoptosis; Bcl-G; Bcl-2 family
Abbreviations: BH, Bcl-2 homology domain; cDC, conventional dendritic cell; pDC, plasmacytoid dendritic cell; HA, haemagglutinin; mAb, monoclonal antibody; DMEM, Dulbecco's modified Eagle's medium; Y2H, yeast two-hybrid; TRAPP, transport particle protein
Received 25.7.12; accepted 25.7.12; Edited by G Melino

Results

Generation of Bcl-G-deficient mice. Targeting of the mouse *Bcl-G* gene in embryonic stem (ES) cells was achieved by introducing loxP sites flanking the ATG-containing exon 3 (Figure 1a). Hygromycin-resistant Bruce 4 clones were isolated and their genomic DNA analysed by Southern blotting (Figure 1b). *Bcl-G* gene-targeted mice were established and maintained on an inbred C57BL/6 genetic background, and were genotyped by PCR (Figure 1c). *Bcl-G*$^{-/-}$ mice were born at the expected Mendelian frequency from intercross matings of *Bcl-G*$^{+/-}$ mice (Figure 1d). The general appearance and behaviour of these mice was normal and they were indistinguishable from their wild-type (WT) littermates.

As expected, no RNA could be detected by RT-PCR in tissues from *Bcl-G*$^{-/-}$ mice (Figure 2a). Our mAb (clone 2E11) detected a 38-kDa band in WT testis, and this band was absent from *Bcl-G*$^{-/-}$ testis (Figure 2b). Interestingly, only one Bcl-G isoform is produced from the mouse *Bcl-G* gene, whereas a long (BCL-G_L) and a short (BCL-G_S) isoform are produced from human *BCL-G*.[4] In the testis, Bcl-G immunoreactivity was limited to the late-stage spermatids within the seminiferous tubules (Figure 2c). No staining was seen in the mature sperm found in the epididymal tubules (data not shown). Interestingly, Bcl-G-deficient male (and female) mice exhibited normal reproductive behaviour and produced litters of normal size.

Bcl-G is expressed in diverse mouse tissues but is not required for their development and function. In addition to the male reproductive organs, high levels of mBcl-G were also found in the thymus, small intestine and colon. Intermediate expression levels were seen in pancreas, spleen and lung, whereas little or no Bcl-G expression was observed in the brain, kidney and liver (Figure 3a). Mouse Bcl-G protein is most similar to human BCL-G_L, and its expression closely matches what is known for h*BCL-G*$_L$ mRNA.[4]

Bcl-G expression was high in many epithelial cells, in particular those lining the gastrointestinal tract and the lumen of mammary ducts (Figure 3b and data not shown). However, no obvious defects were found in these organs in *Bcl-G*$^{-/-}$ mice. *Bcl-G*$^{-/-}$ intestines had similar lengths of villi and crypt depths as those from WT mice (Figure 3b). The numbers of Paneth and goblet cells were also normal, indicating that Bcl-G is not required for intestinal epithelial differentiation (data not shown). In the mammary gland, Bcl-G loss did not affect ductal morphogenesis, and the lumens of ducts in *Bcl-G*$^{-/-}$ females were clear and well developed (Figure 3b). As the survival and growth of pups from litters of *Bcl-G*$^{-/-}$ females was no different from those of WT mothers, we conclude that Bcl-G deficiency did not significantly affect mammary development during pregnancy, nor did it affect milk production or nursing behaviour (data not shown).

Bcl-G is expressed by dendritic cells. Bcl-G was expressed in large cells within the thymic medulla and the centre of lymphocytic follicles of the spleen and lymph nodes (Figure 3b, and data not shown). No significant Bcl-G staining was detected in lymphocytes. The Immunological Genome Project gene expression database revealed high expression of *Bcl-G* mRNA in CD8$^+$ dendritic cells (DCs).[6] We examined Bcl-G expression in select DC subsets from WT spleen using our Bcl-G-specific antibodies (Figure 3c). In accordance with the mRNA expression results, conventional DCs (cDCs; CD11c^{hi} CD45RA$^-$) had significantly higher levels of Bcl-G than plasmacytoid DCs (pDCs; CD11c^{int} CD45RA$^+$) (Figure 3c). This high expression was largely contributed by the CD8$^+$ cDC subset, although Bcl-G was also present at lower levels in the CD4$^+$ and double negative cDC subsets (Figure 3c). Bcl-G expression was increased in splenic cDCs upon stimulation with CpG oligonucleotides, perhaps indicating a role for Bcl-G in the Toll-like receptor 9 signalling pathway (Figure 3c).

The thymic medulla contains epithelial cells that are present in close proximity to the thymic DCs. As Bcl-G displayed expression in certain epithelial cell types in other organs, we investigated whether it is present in medullary thymic epithelial cells. However, double immunofluorescence staining for Bcl-G and the medullary thymic epithelial cell marker keratin-5 on WT thymus sections did not show any colocalisation, demonstrating that the DCs must constitute the majority of the Bcl-G-expressing cells in the thymus (Supplementary Figure 1).

Bcl-G$^{-/-}$ mice have normal haematopoietic cell subset composition. To investigate the impact of Bcl-G loss on the haematopoietic compartment, we analysed the cellular composition of blood, thymus and spleen in adult Bcl-G-deficient mice (Figures 4a–c). Overall numbers of red blood cells, white blood cells and platelets were all normal in Bcl-G-deficient mice (Figure 4a and data not shown). Similarly, thymi and spleens of *Bcl-G*$^{-/-}$ mice had similar weights and total cellularities as those of WT mice (Supplementary Figure 2, and Figures 4b and c). *Bcl-G*$^{-/-}$ mice also had normal numbers of each of the major thymic and splenic subpopulations analysed, showing that loss of Bcl-G did not affect the development and homeostasis of the mouse haematopoietic system (Figures 4b and c).

Bcl-G is dispensable for splenic DC development and apoptosis. As Bcl-G is highly expressed in DCs, particularly the CD8$^+$ subtype, we next measured the numbers of the various splenic DC subsets in *Bcl-G*$^{-/-}$ mice using flow cytometry (Figure 4d and Supplementary Figure 3). The numbers of *Bcl-G*$^{-/-}$ DCs were comparable to those in WT mice (Figure 4d and Supplementary Figure 3). Because of the higher expression of Bcl-G in CD8$^+$ DCs relative to other DC subsets, we also examined the function of the *Bcl-G*$^{-/-}$ CD8$^+$ DCs, using several antigen cross-presentation assays (Supplementary Figure 4). However, neither the *in vivo* cross-presentation assay nor the CTL killing assay revealed any difference between the WT and Bcl-G-deficient DCs, indicating that Bcl-G may not be required for cross-presentation and naive T-cell activation (Supplementary Figure 4).

We next compared the survival of *Bcl-G*$^{-/-}$ and WT DCs in culture (Figure 4e). Splenic DCs from the three subsets (pDC, CD8$^+$ and CD8$^-$ cDC) were purified by FACS and placed in

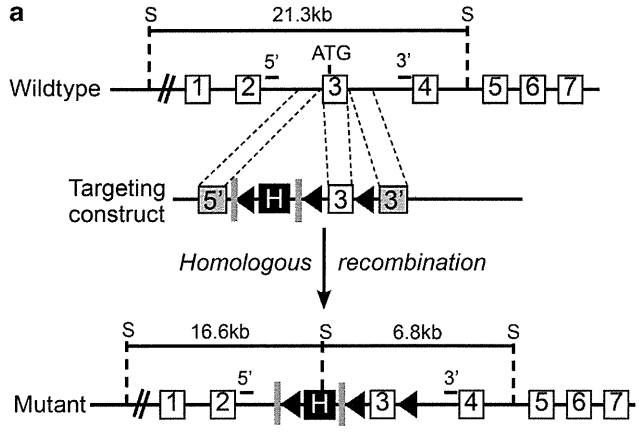

d

	% Offspring from crosses of *Bcl-G*$^{+/-}$ mice (#)		
	Bcl-G$^{+/+}$	*Bcl-G*$^{+/-}$	*Bcl-G*$^{-/-}$
Expected	25% (23)	50% (46)	25% (23)
Actual	37.1% (23)	40.3% (25)	22.6% (14)

Figure 1 Targeting strategy and generation of Bcl-G knock-out mice. (**a**) Schematic diagram depicting the *Bcl-G* locus targeting strategy. Open boxes represent exons and grey boxes represent intronic DNA (corresponding region on WT locus is indicated by dashed lines). H denotes the hygromycin resistance selection cassette (frt/loxP/pGK-Hygro/frt), whereas triangles and rectangles indicate the loxP sites and frt sites, respectively. The locations of the 5′- and 3′-external probes used for Southern blot analysis are shown. (**b**) Southern blot analysis on *Sca*I-digested genomic DNA to identify homologous recombination at the *Bcl-G* locus. Correctly targeted ES cell clones show a 16.6 kb fragment with the 5′-external probe and a 6.8 kb fragment with the 3′-external probe. (**c**) *Bcl-G*$^{-/-}$ mice were identified using a three-primer genotyping PCR protocol on tail DNA. Wild-type mice show a single band of 202 bp, whereas *Bcl-G*$^{-/-}$ mice show a single band of 346 bp. *Bcl-G*$^{+/-}$ mice show both bands. (**d**) Genotypes of offspring produced from crosses of *Bcl-G*$^{+/-}$ mice. The actual numbers are shown in brackets

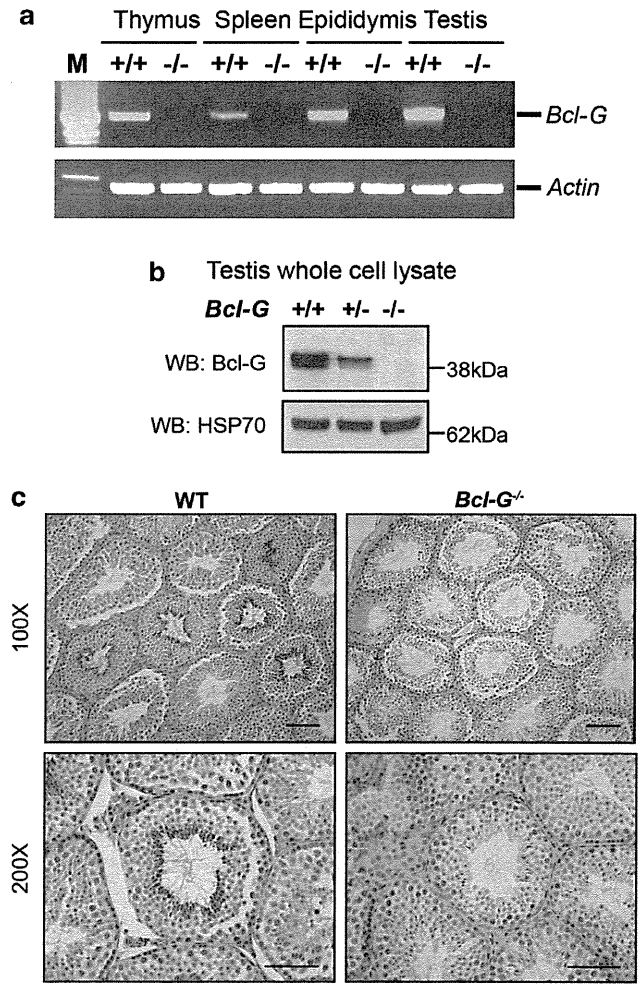

Figure 2 Loss of Bcl-G does not affect testicular development. (**a**) RT-PCR performed on mRNA using inter-exon primers confirmed the absence of functional *Bcl-G* transcripts in tissues of *Bcl-G*$^{-/-}$ mice. PCR using actin-specific primers served as a loading control. (**b**) Western blotting using Bcl-G-specific mAbs detected the presence of Bcl-G protein in testes of WT and *Bcl-G*$^{+/-}$ mice. No Bcl-G protein was detected in the testis from *Bcl-G*$^{-/-}$ mice. Membranes were reprobed for HSP70 as a loading control. (**c**) Anti-Bcl-G immunohistochemistry revealed that Bcl-G expression is limited to the late stage spermatids within the seminiferous tubules. Representative photomicrographs are shown at $\times$ 100 (bar represents 100 μm) and $\times$ 400 magnification (bar represents 40 μm)

medium with or without the survival factor granulocyte-macrophage colony-stimulating factor (GM-CSF; 10 ng/ml). Consistent with previous reports,[7,8] WT DCs, particularly the pDC subtype, underwent rapid cell death *in vitro*, with only ~20% pDCs surviving after 24 h in culture (Figure 4e). There was no significant difference in the rate of death of *Bcl-G*$^{-/-}$ DCs from any of the three subtypes when compared with their WT counterparts (Figure 4e). These results demonstrate that Bcl-G is not required for spontaneous DC apoptosis, both in the presence or absence of GM-CSF. Transient overexpression of mouse Bcl-G did not cause significant killing of 293T cells (Supplementary Figure 5A), further indicating that mBcl-G lacks significant pro-apoptotic activity.

Bcl-G does not bind strongly to the prosurvival Bcl-2-like proteins. The complex interactions between three major subgroups of the Bcl-2 family determine whether apoptosis is activated or not.[9,10] Human BCL-G_S was reported to bind BCL-X_L through its BH3 domain, whereas the presence of the additional BH2 domain in hBCL-G_L was suggested to prevent its binding to BCL-X_L.[4] As mBcl-G is most similar to hBCL-G_L, and as we could not find any evidence that mBcl-G exerted significant proapoptotic activity, we investigated whether it could even bind to the antiapoptotic Bcl-2 family members or Bax/Bak. Haemagglutinin (HA)-tagged mBcl-G was transiently overexpressed together with Flag-tagged prosurvival proteins (Bcl-2, Bcl-x_L, Bcl-w, Mcl-1 and A1), Flag-Bax, Flag-Bak or empty vector as a negative control (Figure 5a). Bcl-G could bind weakly to all

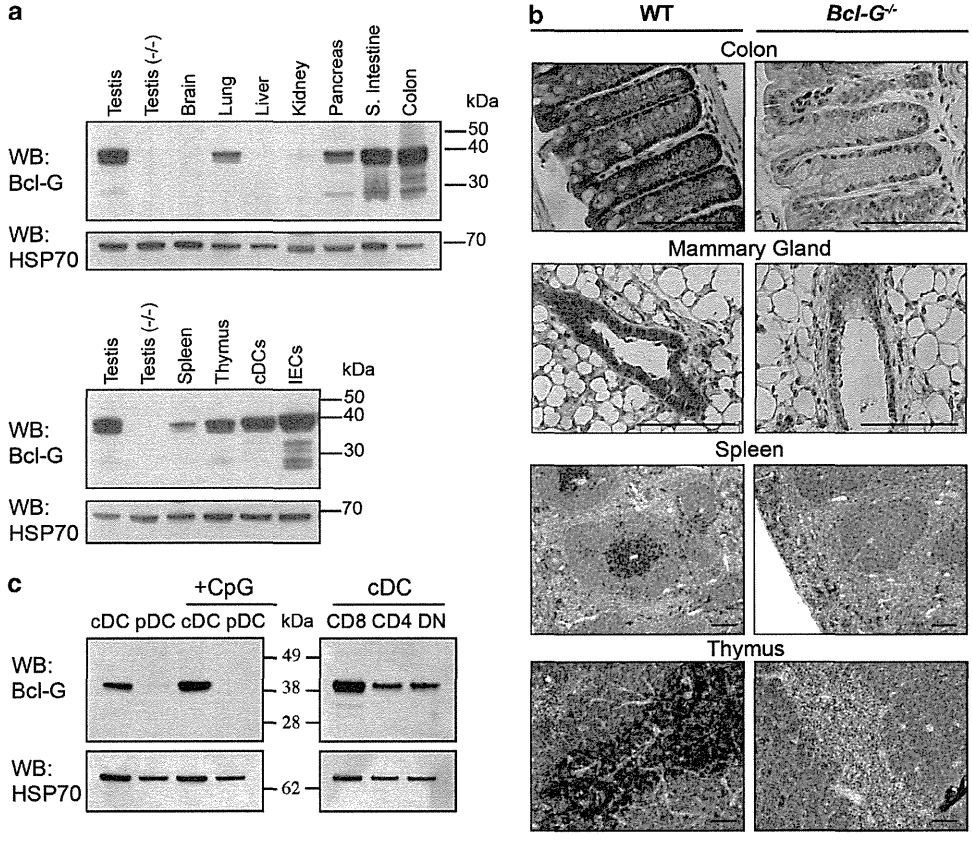

Figure 3 Bcl-G is expressed in epithelial cells in a wide range of tissues and in DCs in the haematopoietic organs. (**a**) Western blot analysis of organs from C57BL/6 (WT) mice to determine distribution of Bcl-G. cDCs indicate FACS-sorted splenic conventional DCs ($CD11c^{hi}$ $CD45RA^{-}$), whereas IECs denote IECs isolated from WT intestines. Lysates from testis of *Bcl-G*$^{-/-}$ mice were used as a negative control. The membranes were reprobed for HSP70 as a loading control. (**b**) Immunohistochemistry using specific mAbs revealed cell type-specific expression of Bcl-G in the colon, mammary gland, spleen and thymus. Tissue sections from *Bcl-G*$^{-/-}$ mice were used as negative controls. The bars represent 100 μm. (**c**) Bcl-G expression in the various splenic DC subsets was analysed by western blotting. pDC stands for plasmacytoid DC ($CD11c^{int}$ $CD45RA^{+}$); CD8, CD4 and double negative (DN) indicates $CD8^{+}$ $CD4^{-}$, $CD8^{-}$ $CD4^{+}$ and $CD8^{-}$ $CD4^{-}$ cells, respectively). Bcl-G content in DCs stimulated with CpG DNA for 24 h was also analysed by western blotting

five prosurvival Bcl-2 family members when they were overexpressed (Figure 5a and Supplementary Figure 5B). In contrast, there was no evidence for significant interaction between mBcl-G and Bax or Bak (Figure 5a).

To determine the role of the BH3 domain in this weak binding, we generated several mutants of mBcl-G, including one lacking the entire BH3 domain (ΔBH3), one in which the conserved leucine within the BH3 domain was changed to alanine (L217A) and one which had the conserved glutamine and aspartate residues mutated to alanine (Figure 5b). Unexpectedly, these mutant Bcl-G proteins retained the ability to interact weakly with Bcl-x_L and all four other prosurvival proteins (Figure 5b and data not shown). These results indicate that Bcl-G might not bind to the prosurvival Bcl-2 family members in the same manner as the canonical BH3-only proteins, such as Bim or Puma. In accordance with what was reported for hBCL-G_L,[4] removal of the BH2 domain from mBcl-G increased its binding to Bcl-x_L (Figure 5b and Supplementary Figure 5B).

To further examine the ability of the BH3 domain of mBcl-G to bind to the prosurvival Bcl-2 family members, we generated a mutant form of Bim_S in which the BH3 domain was replaced with the BH3 domain of mBcl-G, and tested its binding to Bcl-x_L (Figure 5c). This experiment revealed that Bim_S(Bcl-G BH3), such as Bim_S(4E), a well-described non-Bcl-x_L-binding mutant of Bim_S,[11] did not bind Bcl-x_L (Figure 5c). This indicated that the BH3 domain of Bcl-G might be incapable of binding to the prosurvival Bcl-2 family members. Indeed, replacement of the BH3 domain of Bim with that of Bcl-G also resulted in complete loss of Bim's killing potential when overexpressed in 293T cells (Supplementary Figure 5A). Finally, we were unable to observe any endogenous binding of Bcl-G to Bcl-x_L, Bcl-2 and Mcl-1 in mouse tissue (testis, thymus or spleen) protein lysates when we immunoprecipitated either Bcl-G or Bcl-x_L (Supplementary Figure 6). Collectively, these observations suggest that Bcl-G might not function as a classical BH3-only protein.

Novel potential interacting partners for Bcl-G. We then conducted a proteomic screen to identify potential new interacting partners for Bcl-G and thus gain clues on a possible alternative function. The strategy is depicted in Figure 6. Whole-cell lysates were prepared from intestinal epithelial cells (IECs) isolated from WT or *Bcl-G*$^{-/-}$ mice. The presence of Bcl-G in the lysates from the WT cells but not in those from the control (*Bcl-G*$^{-/-}$) cells was verified by

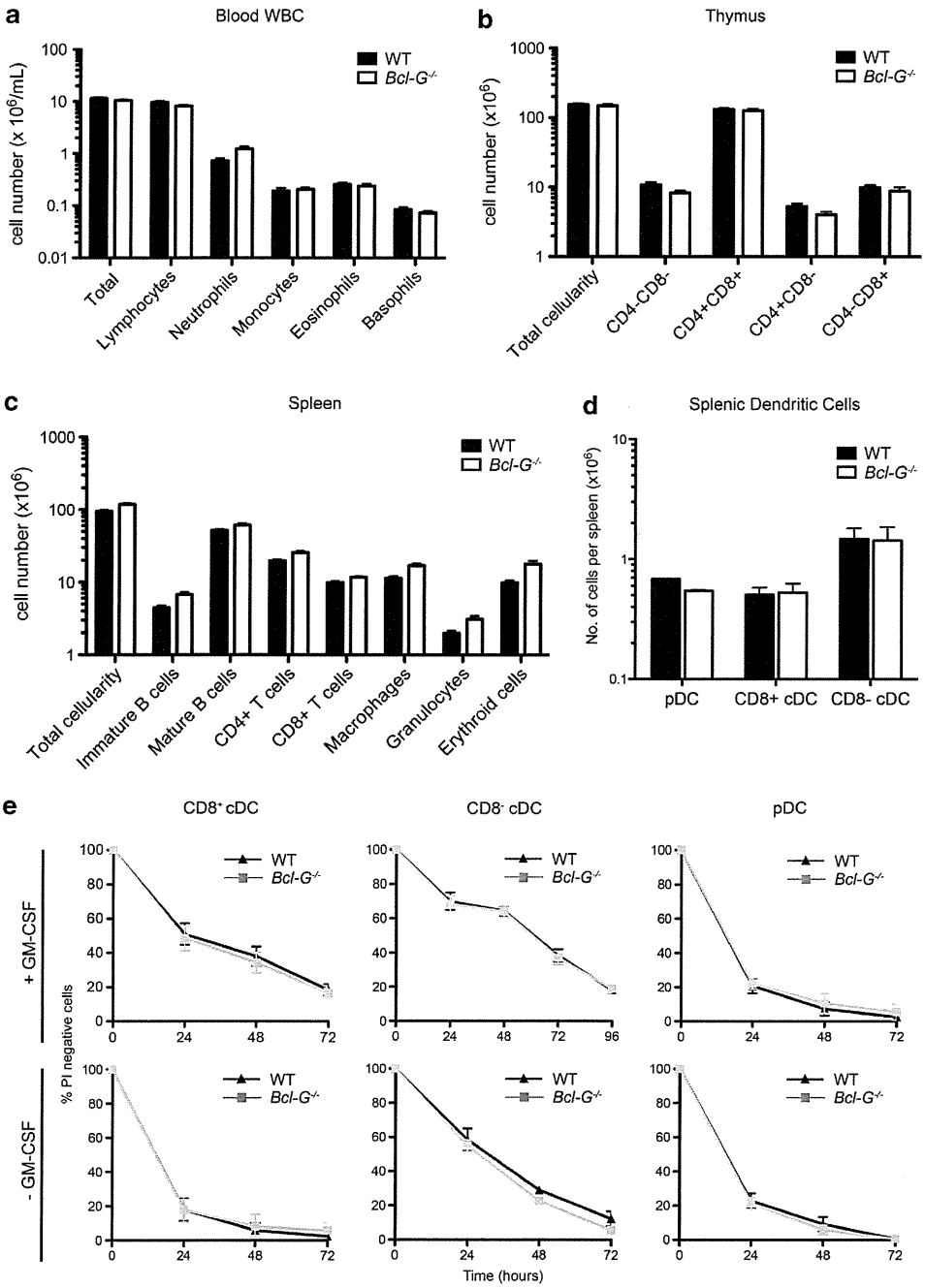

Figure 4 *Bcl-G*$^{-/-}$ mice have normal haematopoietic cell subset composition, and Bcl-G deficiency does not protect splenic DCs from apoptosis. (**a**) Leukocyte cell subset composition of 8–12-week-old WT and *Bcl-G*$^{-/-}$ mice was determined using an ADVIA blood analyser. Single-cell suspensions made from (**b**) thymi and (**c**) spleens of these mice were analysed by FACS after staining with antibodies against various cell surface markers to determine the numbers of the indicated cell subpopulations. Splenic subsets determined included B220^{+}sIgM^{hi}sIgD^{lo} immature B and B220^{+}sIgM^{lo}sIgD^{hi} mature B cells, Mac-1^{+}Gr-1^{-} macrophages, Mac-1^{+}Gr1^{+} granulocytes and Ter119^{+} nucleated erythroid cells. (**d**) Splenic DC subset composition was determined by flow cytometric analysis. The absolute numbers per spleen of cDC (CD11c^{hi}CD45RA^{-}), pDC (CD11c^{int}CD45RA^{+}), CD8^{+} cDC (gated cDC, CD8^{+}Sirpα^{-}) and CD8^{-} cDC (gated cDC, CD8^{-}Sirpα^{+}) are shown (see Supplementary Figure 3). (**e**) FACS-sorted splenic DC subpopulations from WT and *Bcl-G*$^{-/-}$ mice were plated into 96-well plates with or without addition of the DC survival promoting cytokine GM-CSF. Cell viability was determined at specific time points using propidium iodide staining followed by flow cytometric analysis. Data are presented as percentages of PI^{-} live cells *versus* time. The results shown represent at least three independent experiments ($n=24$ of each genotype). Error bars indicate S.E.M.

western blotting (Supplementary Figure 7). Bcl-G protein complexes were immunoprecipitated from these protein lysates using two different Bcl-G-specific mAbs, 2E11 and 10C9, that recognise different epitopes within the Bcl-G protein (Figure 6). Immunoprecipitates were analysed by mass spectrometry.

A total of 327 unique proteins were identified in this screen (Figure 6). Of these, 216 proteins could be eliminated

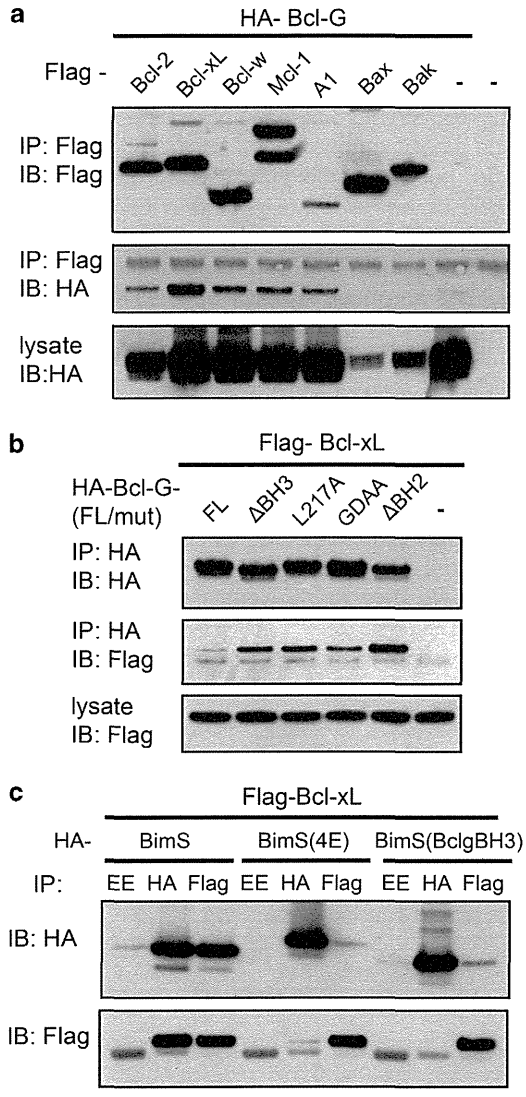

Figure 5 Weak interaction of Bcl-G with prosurvival Bcl-2 family members, which does not require its BH3 domain. Mammalian expression vectors encoding HA- and Flag-tagged proteins were co-transfected into 293T cells: (**a**) Full-length or (**b**) mutant HA-mBcl-G, together with Flag-tagged prosurvival proteins; (**c**) HA-mBim$_S$ (WT or mutant BH3) with Flag-Bcl-x$_L$. Empty HA and Flag vectors were used as negative controls (−). Immunoprecipitations were carried out using Protein G sepharose beads and antibodies against HA, Flag or Glu-glu (negative control). Immunoprecipitates were separated on SDS-PAGE gels and tested for the presence of co-immunoprecipitated Flag- or HA-tagged proteins by western blotting

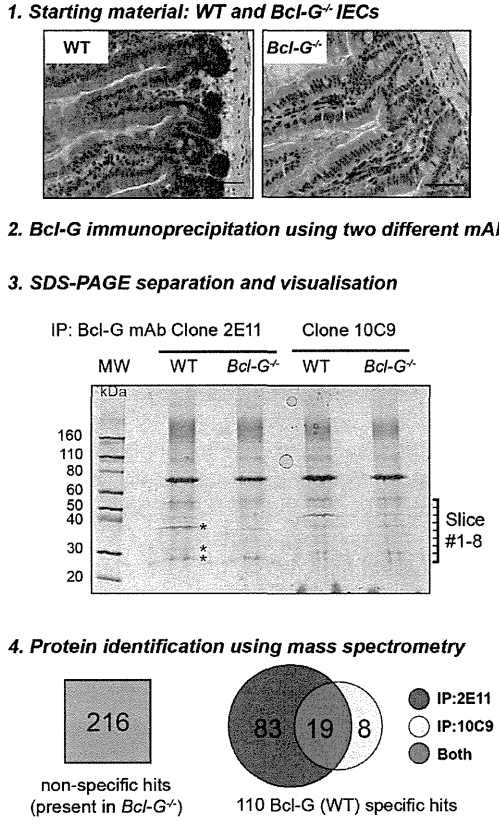

Figure 6 Identification of Bcl-G binding partners using IP–MS proteomic screening. Protein lysates made from IECs of WT or *Bcl-G*$^{-/-}$ mice (**1**) were used to immunoprecipitate Bcl-G using two independent anti-Bcl-G mAbs, 2E11 or 10C9 (**2**). Immunoprecipitated proteins were resolved by SDS-PAGE and visualised by Coomassie brilliant blue staining (**3**). Asterisks indicate the Bcl-G bands present in lane 1 (WT cell lysate, mAb 2E11) but not lane 2 (*Bcl-G*$^{-/-}$ cell lysate, mAb 2E11). Positions of molecular weight markers (MW) are shown. Corresponding regions for each sample were excised, trypsin-digested and sequenced by mass spectrometry (**4**). The 326 proteins identified in the screen were classified by their presence in each sample. Non-specific proteins were identified by their presence in either or both of the pull-downs from *Bcl-G*$^{-/-}$ cell lysates (216 proteins). Potential Bcl-G-interacting partners were identified as being present in either or both of the WT samples and absent in the *Bcl-G*$^{-/-}$ samples (110 proteins)

as non-specific interactors, as they were found in all the samples, including immunoprecipitates from *Bcl-G*$^{-/-}$ cells. As expected from the western blots, Bcl-G-derived peptides were only found in the WT samples (Supplementary Figure 8). A total of 110 unique proteins that potentially interact with Bcl-G were identified (Figure 6 and Supplementary Figure 9). Of these, 19 proteins were found in immunoprecipitates with both antibodies (Figure 6 and Supplementary Figure 9D). Notably, none of the Bcl-2 family members were identified in this screen, consistent with our overexpression/co-immunoprecipitation studies (Figure 5).

Yeast two-hybrid screening identifies Trappc6b as a Bcl-G-binding protein. We reasoned that an independent approach would help to validate and strengthen the results of the IP–MS experiment. We therefore used full-length Bcl-G as a bait to perform a yeast two-hybrid (Y2H) screening of a normalised mouse universal cDNA library (Clontech, Mountain View, CA, USA). In a screen of approximately 3×10^6 transformants, we obtained 52 colonies growing on plates containing selective medium. Of the cDNAs picked up in this screen, three were in the correct reading frame. cDNAs encoding the transport particle protein (TRAPP) complex 6b (Trappc6b) represented 19 of the 52 isolated clones. The other clones encoded parts of Sorting nexin 14 (Snx14) and Transmembrane protein 167B (Tmem167B) and were each found once. Importantly, none of the Bcl-2 family members were pulled down as potential Bcl-G-binding partners in this screen. In addition, mBcl-G did

not appear to bind to itself when overexpressed, in contrast to a previous report.[12]

Out of the three potential hits, we focused our attention on Trappc6b, as three components of TRAPP complexes (Trappc3, Trappc4 and Trappc5) had been identified in the IP–MS experiment (Table 1). To confirm the Y2H screening results, we introduced the pGADT7–Trappc6b plasmid into the AH109 yeast strain together with bait plasmid pGBT9–Bcl-G (FL) or pGBT9 vector alone (V; Figure 7a). Only yeast cells transformed with both Trappc6b, and Bcl-G survived on -Leu-Trp-His-Ade plates and turned blue in the X-gal assay that detects the presence of α-galactosidase activity (Figure 7a). This interaction was specific, as deleting particular regions (amino acids 103–136 and 273–328) of the Bcl-G protein resulted in lack of α-galactosidase activity and no growth on the selective plates (Figure 7a and Supplementary Figure 10). In a pull-down experiment, ectopically expressed Flag–Trappc6b was found to bind to His-tagged Bcl-G, immobilised on Ni-NTA agarose beads (Figure 7b).

Collectively, the results from the Y2H screen and the IP–MS experiment confirm that Bcl-G does not bind significantly to other members of the Bcl-2 family and strongly suggest that it is involved in vesicle trafficking and protein transport across the cells by interacting with the TRAPP complex.

Discussion

Proteins of the Bcl-2 family are characterised by the presence of BH domains that are important in determining the three-dimensional structure of these proteins and their interactions with the other members of the family. In this regard, mBcl-G and its human homologue BCL-G_L are rather unique members of the Bcl-2 family, as they contain both BH3 and BH2 domains.[4,5] The only other protein in this family to contain such a combination of BH domains is Bfk.[13] Overexpression of hBCL-Gs was found to induce apoptosis in certain cell lines, whereas hBCL-G_L did not.[4] Accordingly, *BCL-G* is widely (if not universally) considered to encode yet another proapoptotic BH3-only protein, but this proapoptotic activity has not been confirmed in an independent study, let alone within a physiological context. A database search indicated that the BCL-G_S isoform only exists in humans, as the alternative splice acceptor site that is used to produce it is not conserved in other species. In accord with its lack of killing activity (even when overexpressed), hBCL-G_L did not bind BCL-X_L.[4] Although we detected a weak interaction of mBcl-G with several prosurvival Bcl-2 family members, this interaction was still observed when the BH3 domain of Bcl-G was mutated or removed. In fact, closer examination indicates that the BH3

Table 1 Trapp complex subunits identified as potential mouse Bcl-G-binding partners in the IP–MS proteomic screen

Acc. no.	Gene symbol	Protein name	No of peptides	% Coverage
Q9ES56	*Trappc4*	Trafficking protein particle complex subunit 4	2	11.00
Q9CQA1	*Trappc5*	Trafficking protein particle complex subunit 5	2	9.57
O55013	*Trappc3*	Trafficking protein particle complex subunit 3	2	12.80

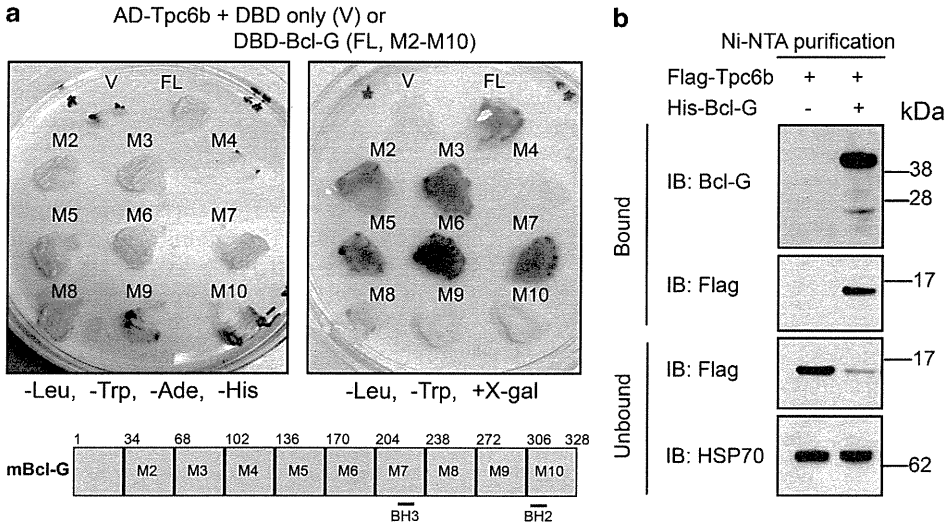

Figure 7 Trappc6b interacts with mBcl-G in the Y2H assay. (**a**) pGBT9-DBD empty vector or pGBT9-DBD-mBcl-G (full-length and truncation mutants M2–M10) were co-transformed with pGADT7-AD-Trappc6b into the yeast strain AH109. Positive interactions were tested by streaking transformants onto a -Leu-Trp-His-Ade plate (left) and the β-galactosidase assay was performed using X-gal staining of yeasts growing on a -Leu-Trp plate (right panel). The amino acid positions of the truncations within the Bcl-G mutants are shown in the schematic below. See Supplementary Figure 9 for more details. (**b**) Cell lysates made from 293T cells overexpressing Flag-Trappc6b were added to Ni-NTA beads pre-incubated with recombinant His-mBcl-G purified from *Escherichia coli*. Flag-Trappc6b bound to immobilised Bcl-G was identified by anti-Flag western blotting. Detection of unbound Trappc6b in the control sample indicates input. Probing for HSP70 served as a control that equal amounts of protein lysates were used

domain of Bcl-G does not conform to the BH3 consensus sequence; for example, the uniformly hydrophobic residue in position Φ3 is replaced with a serine (S220). This may explain why mBcl-G binds poorly to prosurvival family members. Strikingly, no Bcl-2 family member, prosurvival or proapoptotic, was pulled down in either our proteomic screen or the Y2H screen. Collectively, these results indicate that mBcl-G is most likely not involved in interactions with other Bcl-2 family members and, therefore, probably does not function in the intrinsic apoptotic pathway.

To determine which tissues and cell types normally express Bcl-G, we have generated three highly specific mAbs.[14] In western blots, mBcl-G appears as a ~38-kDa band that is not present in *Bcl-G*$^{-/-}$ animals. It is worth noting that some of the earliest commercially available anti-BCL-G antibodies detect a single ~22-kDa band that corresponds neither to the size of hBCL-G_L nor that of hBCL-G_S. We found that Bcl-G is highly expressed in many epithelial cells, as well as in DCs. This guided the choice of the source of protein lysates for our IP–MS experiment, as we wanted to avoid using Bcl-G overexpression. Our search for novel interacting partners using two independent approaches led to the discovery that Bcl-G may be a component of the TRAPP complex, which is involved in vesicle-mediated protein transport. Two large multi-subunit TRAPP complexes have been identified in yeast, whereas there seems to be only one TRAPP complex in mammals.[15] These complexes function in the endoplasmic reticulum (ER) to Golgi transport, as well as intra-Golgi transport. Our immunofluorescence studies did not reveal any specific subcellular localisation of Bcl-G in the Golgi, ER or within vesicular structures when overexpressed in HeLa cells.[14] However, Bcl-G overexpressed in HeLa cells may not reflect its physiological localisation as it was shown in the case of Trapp complex subunit 3.[16] As Bcl-G does not exist in yeast, it is difficult to predict what its precise function in the TRAPP complex is, and more work is required to determine this function.

The *BCL-G* gene is located on human chromosome region 12p12–13, which has been associated with a range of malignancies.[17] A search for a putative prostate cancer tumour suppressor gene within this region revealed that *Bcl-G* transcript levels were downregulated in tumour samples compared with normal prostate tissue.[18] No mutations or expression changes of the *Bcl-G* gene were found in children with acute lymphoblastic leukaemia,[17] but a TEL–AML1 fusion transcript involving *BCL-G* was reported in another.[19] In breast cancer, Bcl-G expression was found to be abnormally reduced and possibly regulated post-translationally by maternal embryonic leucine zipper kinase, a recently identified protein kinase and candidate oncoprotein upregulated in several types of cancer.[20] In all these studies, BCL-G was considered a proapoptotic BH3-only protein and, as such, a potential tumour suppressor. These considerations must now be revised in the light of our results, which show that Bcl-G is not an inducer of apoptosis, although they do not preclude by any means that BCL-G may still work as a tumour suppressor. Hence, the importance of Bcl-G in initiation and progression of cancer remains to be studied.

Certain cell types with prominent Bcl-G expression were studied in detail in an attempt to identify a defect caused by the loss of this protein. Most DCs have a short lifespan, and upon activation and antigen presentation, they rapidly undergo apoptosis to limit the potency of the immune response that had been elicited.[8,21] Members of the Bcl-2 protein family have critical roles in DC apoptosis.[21–23] For example, DCs from *Bim*$^{-/-}$ mice are abnormally resistant to spontaneous apoptosis, leading to enhanced T-cell activation and autoantibody production *in vivo*.[7,24] In contrast, loss of Bcl-G did not impact on DC lifespan, nor did it significantly impact on their main functions, such as antigen cross presentation.

The lack of an obvious phenotype in Bcl-G-deficient mice could be attributed to the existence of functional redundancy, as was reported for other members of the Bcl-2 protein family.[25] However, our results have indicated that Bcl-G might not have a proapoptotic function after all. It thus seems reasonable to investigate the function of Bcl-G further before embarking on time-consuming and costly double-knockout studies.

Several BH3 domain-containing proteins have been shown to function outside the conventional Bcl-2-regulated apoptotic pathway, including cell cycle control, autophagy, calcium homeostasis and ER morphogenesis.[3] It appears likely that Bcl-G may have to be added to this list. The Bcl-G-deficient mice as well as the mAbs that we have generated should prove valuable tools to further study this intriguing Bcl-2 family member.

Materials and Methods

Generation of Bcl-G$^{-/-}$ mice. The targeting construct was designed to introduce loxP sites on either side of the ATG start codon containing exon 3, as well as an FRT-flanked PGK-hygromycin resistance cassette for screening purposes. The targeting construct was electroporated into C57BL/6-derived Bruce-4 ES cells.[26] Homologous recombination events were identified by Southern blotting, using external 5′- and 3′-genomic probes, and blotting with a hygro-specific probe confirmed single-construct integration. Two correctly targeted ES cell clones were injected into blastocysts, resulting in two independent *Bcl-G* gene-targeted mouse strains. Exon 3 and the hygromycin-resistance cassette were deleted by crossing the resultant *Bcl-G*$^{loxP/wt}$ heterozygous mice with C57BL/6 cre deleter mice, and the Cre transgene was subsequently eliminated by crossing offspring to C57BL/6 mice. All of the mice analysed were devoid of hygro and cre. Genotyping of Bcl-G-deficient mice was performed using a three-primer PCR reaction using a common forward primer (5′-TCCGTCCCATTATAACCCTA-3′), together with two reverse primers (5′-CTGGAACGACAGAGGGCAAA-3′ and 5′-TTACCATCACAGAGCCAGAA-3′). The WT and mutant alleles produced products of 202 and 346 bp, respectively.

C57BL/6, B6.CH-2bm 1 (*bm1*) and OT-I[27] mice were obtained from WEHI Bioservices (Kew, VIC, Australia). All animal procedures were reviewed and approved by the Melbourne Directorate Animal Ethics Committee.

RT-PCR analysis. RNA extraction was performed with the TRIzol method (Life Technologies, Mulgrave, VIC, Australia) according to the manufacturer's instructions. cDNA was synthesised using the TaqMan Gold RT-PCR kit (Life Technologies). The PCR amplification step used GoTaq Green Master Mix (Promega, Alexandria, NSW, Australia) and 25 pmol of each forward (5′-CCCAAGCTCTCCAGAACAAG-3′) and reverse (5′-CAGCAGCTCAACAATCTTGC-3′) primers.

Western blotting and immunoprecipitation. HEK293T cells were maintained in Dulbecco's modified Eagle's medium (DMEM) supplemented with 10% fetal bovine serum, transiently transfected using Fugene 6 reagent (Roche, Dee Why, NSW, Australia), and were harvested 40 h post-transfection. Cells were lysed in 20 mM Tris-pH 7.4, 135 mM NaCl, 1.5 mM MgCl2, 1 mM EGTA, 10% glycerol and 1% Triton X-100 supplemented with complete protease inhibitor cocktail tablets (Roche). Lysates were incubated with protein G-sepharose beads and antibodies against HA (3F10; Roche), Flag (M2; Sigma-Aldrich, Rowville,

VIC, Australia) or EE (Glu-Glu; Covance, North Ryde, NSW, Australia). Protein complexes were resolved on 4–12% Bis-Tris SDS-PAGE gels (Life Technologies) and detected on western blots with rat mAbs to Bcl-G (2E11)[14] or HA and mouse mAbs to Flag (M2, Sigma-Aldrich), HSP70 (N6; a kind gift from Dr R Anderson, Peter MacCallum Cancer Research Centre, Melbourne, VIC, Australia) or Actin (AC-40; Sigma-Aldrich). Labelled protein bands were detected by incubation with goat anti-mouse Ig or goat anti-rat IgG antibodies conjugated to horseradish peroxidase (Southern Biotech, Birmingham, AL, USA), followed by chemiluminescence analysis (ECL; GE Healthcare, Rydalmere, NSW, Australia)

Histology and tissue immunohistochemistry. Mouse tissues were fixed in 10% formalin. Protocols used for immunohistochemistry and immunofluorescence have been described.[14]

Immunofluorescence and flow cytometric analysis. Peripheral blood was analysed with the ADVIA 120 Hematology System (Bayer, Tarrytown, NY, USA). Single-cell suspensions prepared from thymi and spleens were counted using the CASY Cell Counter (Roche). Cells were stained for flow cytometric analysis using fluorochrome (fluorescein isothiocyanate, PE, APC or PerCP)-conjugated antibodies to Thy1.2 (T24.31.2), CD8 (YTS169), B220 (RA3-6B2), IgM (5.1), IgD (1126C), Gr-1 (8C5), CD3 (KT3-1.1), CD4 (YTA-321), CD11b (Mac-1) and Ter-119 (erythroid cell marker). Staining with propidium iodide (5 μg/ml) was used to label dead cells. Data were acquired on either a FACScan or an LSR II flow cytometer (BD Biosciences, San Jose, CA, USA). All data analysis was performed using FlowJo software (TreeStar, Ashland, OR, USA).

DC isolation and treatments. DCs were isolated from spleens of mice according to previously published protocols,[28] followed in some cases by high-speed cell sorting (MoFlo, Cytomation, Fort Collins, CO, USA). DC populations purified from WT or *Bcl-G*$^{-/-}$ mice were added to 96-well plates at 1×10^5 cells per well in RPMI medium 1640 supplemented with 10% FCS, 50 μM 2-mercaptoethanol, 2 mM L-glutamine, 100 units/ml penicillin, 100 μg/ml streptomycin with or without supplementation with 100 ng/ml GM-CSF (PeproTech, Rocky Hill, NJ, USA) and/or 0.5 μM CpG_{1168} (Geneworks, Hindmarsh SA, Australia). *In vivo* OT-I TCR transgenic T-cell proliferation assays and *in vivo* CTL assays were performed as described.[29]

Isolation of primary small IECs. Small intestines from either WT or *Bcl-G*$^{-/-}$ mice were removed, opened longitudinally, cut into 0.5-cm pieces and placed into ice-cold DMEM media containing 1 mM DTT. Gut pieces were shaken gently for 15 min at 37 °C, the dislodged cells filtered out and solid material placed in PBS solution containing 15 mM EDTA, followed by a further 10-min incubation with shaking at 37 °C. After vortexing to dislodge IECs, cell suspensions were passed through cell strainers (100 μm, BD Biosciences) and centrifuged at 4 °C at $300 \times g$ for 5 min.

Mass spectrometry. Immunoprecipitates were resolved on a 4–12% Bis-Tris SDS-PAGE gel (Invitrogen, Grand Island, NY, USA) and visualised by staining with the Colloidal Blue Staining Kit (Invitrogen). The gel regions between 25–55 kDa were excised and divided into eight equal slices, which were then subjected to in-gel reduction, alkylation and tryptic digestion. Extracted peptides were injected and fractionated by nanoflow reverse-phase liquid chromatography on a nano LC system (1200 series; Agilent, Santa Clara, CA, USA). The nano HPLC was coupled online to an LTQ-Orbitrap mass spectrometer equipped with a nanoelectrospray ion source (Thermo Fisher Scientific, Scoresby, VIC, Australia) for automated MS/MS. For protein identification within gel samples, LC-MS/MS data were searched against a non-redundant protein decoy database comprising sequences from the latest version of LudwigNR (Mouse Species, Melbourne, VIC, Australia). Mass spectra peak lists were extracted using extract-msn as part of Bioworks 3.3.1 (Thermo Fisher Scientific) linked into Mascot Daemon (Matrix Science, London, UK). Peak lists for each nano-LC-MS/MS run were used to search MASCOT v2.2.04 search algorithm (Matrix Science) provided by the Australian Proteomics Computational Facility (www.apcf.edu.au).

Y2H assay. A pre-transformed normalised Matchmaker mouse universal cDNA library prepared with pGADT7-RecAB was purchased from Clontech and screened by the Matchmaker GAL4 Two-Hybrid System (Clontech) according to the manufacturer's protocol. Full-length *mBcl-G* cDNA fragment was amplified by PCR and cloned into pGBT9 (Clontech). The yeast *Saccharomyces cerevisiae* strain AH109 (maintained in YEPD medium), which secretes α-galactosidase under the control of the MEL1 region, was transformed with pGBT9-mBcl-G and grown on a medium lacking tryptophan. The clone including the bait plasmid was transformed with the library plasmids. The transformed yeast cells were grown on 2% agar plates of a dropout medium lacking tryptophan, leucine, histidine and adenine (-Leu-Trp-His-Ade). The resulting colonies grown on the drop-out plate were inoculated again on a new drop-out plate containing 20 μg/ml X-α-Gal (5-bromo-4-chloro-3-indolyl-α-*O*-galactopyranoside; Clontech) and incubated at 30 °C for 7 days. Yeast co-transformed with pGADT7 and pGBT9 empty vectors, or pGBT9-p53 and pGADT7-LgT were used, respectively, as negative and positive controls. Total DNA was prepared from all positive blue colonies and introduced into *E. coli* TOP10 competent cells (Invitrogen). The prey plasmids were recovered and sequenced.

Ni–NTA agarose purification. Forty-eight hours post-transfection, 293T cells were washed with PBS and resuspended in onyx lysis buffer. Ni–NTA agarose beads (20 μl) (Qiagen, Chadstone, VIC, Australia) pre-incubated for 1 h with recombinant His-Bcl-G protein (12 μg) were washed, added to cell extracts and rotated at 4 °C for 2 h. Precipitates were washed four times with lysis buffer and then boiled in 40 μl 2 × NuPAGE LDS buffer (Invitrogen) followed by SDS-PAGE analysis.

Data analysis. All graphing and statistical analyses were performed using the Prism v4.0 (GraphPad Software, San Diego, CA, USA).

Conflict of Interest

The authors declare no conflict of interest.

Acknowledgements. We thank M Robati for technical assistance; LA O'Reilly for sharing reagents and expertise; G Siciliano, J Coughlin, E Sutherland and S O'Connor for mouse care; J Corbin for automated blood analysis; B Helbert and C Young for genotyping; K Wycherley for mAb production; E Tsui, S Mihajlovic and their team for histological preparations; and H Patsiouras and E Kapp from the Joint Proteomics Laboratory for mass spectrometry analysis. This work was supported by the Australian NHMRC (Program Grant 461221, Independent Research Institutes Infrastructure Support Scheme Grant 361646, and a Career Development Award), the Leukemia and Lymphoma Society (Specialised Center of Research Grant 7015), and infrastructure support from the NHMRC (IRISS) and the Victorian State Government (OIS). M Giam was funded by University of Melbourne under the Endeavour IPRS scholarship programme. JD Mintern is the recipient of an NHMRC Career Development Award.

1. Giam M, Huang DC, Bouillet P. BH3-only proteins and their roles in programmed cell death. *Oncogene* 2008; **27**: S128–S136.
2. Hinds MG, Day CL. Regulation of apoptosis: uncovering the binding determinants. *Curr Opin Struct Biol* 2005; **15**: 690–699.
3. Lomonosova E, Chinnadurai G. BH3-only proteins in apoptosis and beyond: an overview. *Oncogene* 2008; **27**: S2–S19.
4. Guo B, Godzik A, Reed JC. Bcl-G, a novel pro-apoptotic member of the Bcl-2 family. *J Biol Chem* 2001; **276**: 2780–2785.
5. Nakamura M, Tanigawa Y. Characterization of ubiquitin-like polypeptide acceptor protein, a novel pro-apoptotic member of the Bcl2 family. *Eur J Biochem* 2003; **270**: 4052–4058.
6. Heng TS, Painter MW. The Immunological Genome Project: networks of gene expression in immune cells. *Nat Immunol* 2008; **9**: 1091–1094.
7. Chen M, Huang L, Wang J. Deficiency of Bim in dendritic cells contributes to overactivation of lymphocytes and autoimmunity. *Blood* 2007; **109**: 4360–4367.
8. Chen M, Huang L, Shabier Z, Wang J. Regulation of the lifespan in dendritic cell subsets. *Mol Immunol* 2007; **44**: 2558–2565.
9. Youle RJ, Strasser A. The BCL-2 protein family: opposing activities that mediate cell death. *Nat Rev Mol Cell Biol* 2008; **9**: 47–59.
10. Strasser A, Cory S, Adams JM. Deciphering the rules of programmed cell death to improve therapy of cancer and other diseases. *EMBO J* 2011; **30**: 3667–3683.
11. Chen L, Willis SN, Wei A, Smith BJ, Fletcher JI, Hinds MG *et al.* Differential targeting of pro-survival Bcl-2 proteins by their BH3-only ligands allows complementary apoptotic function. *Mol Cell* 2005; **17**: 393–403.
12. Liu X, Pan Z, Zhang L, Sun Q, Wan J, Tian C *et al.* JAB1 accelerates mitochondrial apoptosis by interaction with proapoptotic BclGs. *Cell Signal* 2008; **20**: 230–240.
13. Coultas L, Pellegrini M, Visvader JE, Lindeman GJ, Chen L, Adams JM *et al.* Bfk: a novel weakly proapoptotic member of the Bcl-2 protein family with a BH3 and a BH2 region. *Cell Death Differ* 2003; **10**: 185–192.

14. Giam M, Mintern JD, Rautureau GJP, Hinds MG, Strasser A, Bouillet P. Detection of Bcl-2 family member Bcl-G in mouse tissues using new monoclonal antibodies. *Cell Death and Disease* 2012; **3**: e-pub ahead of print 23 August 2012; doi:10.1038/cddis.2012.117.
15. Sacher M, Kim YG, Lavie A, Oh BH, Segev N. The TRAPP complex: insights into its architecture and function. *Traffic* 2008; **9**: 2032–2042.
16. Yu S, Satoh A, Pypaert M, Mullen K, Hay JC, Ferro-Novick S. mBet3p is required for homotypic COPII vesicle tethering in mammalian cells. *J Cell Biol* 2006; **174**: 359–368.
17. Montpetit A, Larose J, Boily G, Langlois S, Trudel N, Sinnett D. Mutational and expression analysis of the chromosome 12p candidate tumor suppressor genes in pre-B acute lymphoblastic leukemia. *Leukemia* 2004; **18**: 1499–1504.
18. Latil A, Bieche I, Chene L, Laurendeau I, Berthon P, Cussenot O *et al.* Gene expression profiling in clinically localized prostate cancer: a four-gene expression model predicts clinical behavior. *Clin Cancer Res* 2003; **9**: 5477–5485.
19. Abdelhaleem M, Yi Q, Beimnet K, Hitzler J. A novel TEL-AML1 fusion transcript involving the pro-apoptotic gene BCL-G in pediatric precursor B acute lymphoblastic leukemia. *Leukemia* 2006; **20**: 1294.
20. Lin ML, Park JH, Nishidate T, Nakamura Y, Katagiri T. Involvement of maternal embryonic leucine zipper kinase (MELK) in mammary carcinogenesis through interaction with Bcl-G, a pro-apoptotic member of the Bcl-2 family. *Breast Cancer Res* 2007; **9**: R17.
21. Kamath AT, Henri S, Battye F, Tough DF, Shortman K. Developmental kinetics and lifespan of dendritic cells in mouse lymphoid organs. *Blood* 2002; **100**: 1734–1741.
22. Nopora A, Brocker T. Bcl-2 controls dendritic cell longevity *in vivo*. *J Immunol* 2002; **169**: 3006–3014.
23. Hon H, Rucker EB III, Hennighausen L, Jacob J. bcl-xL is critical for dendritic cell survival *in vivo*. *J Immunol* 2004; **173**: 4425–4432.
24. Fuertes Marraco SA, Scott CL, Bouillet P, Ives A, Masina S, Vremec D *et al.* Type I interferon drives dendritic cell apoptosis via multiple BH3-only proteins following activation by PolyIC *in vivo*. *PLoS One* 2011; **6**: e20189.
25. Coultas L, Bouillet P, Loveland KL, Meachem S, Perlman H, Adams JM *et al.* Concomitant loss of proapoptotic BH3-only Bcl-2 antagonists Bik and Bim arrests spermatogenesis. *Embo J* 2005; **24**: 3963–3973.
26. Lemckert FA, Sedgwick JD, Korner H. Gene targeting in C57BL/6 ES cells. Successful germ line transmission using recipient BALB/c blastocysts developmentally matured *in vitro*. *Nucleic Acids Res* 1997; **25**: 917–918.
27. Hogquist KA, Jameson SC, Heath WR, Howard JL, Bevan MJ, Carbone FR. T cell receptor antagonist peptides induce positive selection. *Cell* 1994; **76**: 17–27.
28. Vremec D, Pooley J, Hochrein H, Wu L, Shortman K. CD4 and CD8 expression by dendritic cell subtypes in mouse thymus and spleen. *J Immunol* 2000; **164**: 2978–2986.
29. Wilson NS, Behrens GM, Lundie RJ, Smith CM, Waithman J, Young L *et al.* Systemic activation of dendritic cells by Toll-like receptor ligands or malaria infection impairs cross-presentation and antiviral immunity. *Nat Immunol* 2006; **7**: 165–172.

Supplementary information accompanies the paper on Cell Death and Disease website (http://www.nature.com/cddis)

JVI
Journals.ASM.org

Sheeppox Virus SPPV14 Encodes a Bcl-2-Like Cell Death Inhibitor That Counters a Distinct Set of Mammalian Proapoptotic Proteins

Toru Okamoto,[a,b]* Stephanie Campbell,[c] Ninad Mehta,[c] John Thibault,[c] Peter M. Colman,[a,b] Michele Barry,[c] David C. S. Huang,[a,b] and Marc Kvansakul[a]*

The Walter and Eliza Hall Institute of Medical Research, Parkville, Victoria, Australia[a]; Department of Medical Biology, University of Melbourne, Parkville, Victoria, Australia[b]; and Li Ka Shing Institute for Virology, Department of Medical Microbiology and Immunology, University of Alberta, Edmonton, Alberta, Canada[c]

Many viruses express inhibitors of programmed cell death (apoptosis), thereby countering host defenses that would otherwise rapidly clear infected cells. To counter this, viruses such as adenoviruses and herpesviruses express recognizable homologs of the mammalian prosurvival protein Bcl-2. In contrast, the majority of poxviruses lack viral Bcl-2 (vBcl-2) homologs that are readily identified by sequence similarities. One such virus, myxoma virus, which is the causative agent of myxomatosis, expresses a virulence factor that is a potent inhibitor of apoptosis. In spite of the scant sequence similarity to Bcl-2, myxoma virus M11L adopts an almost identical 3-dimensional fold. We used M11L as bait in a sequence similarity search for other Bcl-2-like proteins and identified six putative vBcl-2 proteins from poxviruses. Some are potent inhibitors of apoptosis, in particular sheeppox virus SPPV14, which inhibited cell death induced by multiple agents. Importantly, SPPV14 compensated for the loss of antiapoptotic F1L in vaccinia virus and acts to directly counter the cell death mediators Bax and Bak. SPPV14 also engages a unique subset of the death-promoting BH3-only ligands, including Bim, Puma, Bmf, and Hrk. This suggests that SPPV14 may have been selected for specific biological roles as a virulence factor for sheeppox virus.

Viruses employ diverse strategies to subvert the death of infected host cells by apoptosis (23). The process of determining whether a cell lives or dies is critically dependent on the actions of Bcl-2 protein family members, which are key regulators of the mitochondrial or intrinsic pathway of apoptosis (68). Their central role is reinforced by the realization that certain viruses express sequence, structural, or functional homologs of mammalian Bcl-2 (13). Such members of the wider Bcl-2 family are readily recognizable, as they share one to four regions of sequence similarity, the *B*cl-2 *h*omology (BH) domains. In higher organisms, the prosurvival family members, such as Bcl-2, Bcl-x_L, and Mcl-1, keep cells viable unless they are bound and inactivated by the proapoptotic BH3-only proteins, such as Bim or Bad (44). BH3-only proteins are activated by damage signals triggered after cellular insults, such as growth factor deprivation or exposure to cytotoxic drugs, to initiate the cell death machinery (55). Unlike the prosurvival Bcl-2 proteins, which contain multiple BH domains, the BH3-only proteins contain only an α-helical BH3 domain, which binds a receptor-like groove on the prosurvival proteins (44). The key consequence is to activate the multidomain death mediators Bax and Bak to drive mitochondrial outer membrane permeabilization (MOMP), which results ultimately in the activation of proteolytic enzymes (caspases) that drive cellular demolition (27).

A number of viruses, including adenovirus (66), Kaposi sarcoma-associated herpesvirus (KSHV) (52), Epstein-Barr virus (EBV) (30), fowlpox virus FPV039 (1), and orf virus ORFV125 (64, 65), encode recognizable homologous Bcl-2-like proteins that were recognized by their sequence similarities indicating the presence of one or more BH domains (13). Subsequent structure determination of KSHV Bcl-2 (35) and EBV BHRF1 (36, 41) confirmed that both adopt the classical Bcl-2 fold encompassing the canonical hydrophobic binding groove observed in their cellular counterparts. Notably, viral Bcl-2-like proteins are often required for successful viral propagation, emphasizing the critical role inhibition of host cell apoptosis plays during viral infections (23). However, other viruses express antiapoptotic proteins that appear unrelated by sequence to known cell death regulators. They include myxoma virus-encoded M11L (19, 20, 25), human cytomegalovirus-encoded vMIA (24), murine cytomegalovirus-encoded m38 (38), and vaccinia virus-encoded F1L (21, 48, 49, 61, 63) and N1L (2, 7, 12). Despite the lack of sequence similarity to the Bcl-2 protein family, both F1L and M11L adopt a Bcl-2 fold (16, 40, 42), and the structure of M11L in complex with the BH3 peptide from Bak revealed that M11L binds BH3 ligands via the canonical BH3 binding groove (40). Similar to mammalian cell death antagonists, M11L acts to directly counter the cell death mediators Bax and Bak expressed by the host (40).

Overall, these studies suggest that there may be other yet-to-be-identified viral Bcl-2 proteins, and we embarked on a search for other viral gene products that bear sequence similarity to M11L to sample a different region of sequence space compared to cellular Bcl-2 proteins. Six candidate poxvirus genes were identified using a BLAST search, and one originating from sheeppox virus was selected for further analysis, since it appeared to be as potent an inhibitor of apoptosis as M11L in an initial cell death assay. Sheeppox virus is a member of the genus *Capripoxvirus* within the subfamily *Chordopoxvirus* of the *Poxviridae*. Sheeppox is endemic in

Received 4 May 2012 **Accepted** 24 July 2012
Published ahead of print 15 August 2012
Address correspondence to David C. S. Huang, huang_d@wehi.edu.au, or Marc Kvansakul, m.kvansakul@latrobe.edu.au.
* Present address: Marc Kvansakul, Department of Biochemistry, La Trobe University, Victoria, Australia; Toru Okamoto, Department of Molecular Virology, Research Institute for Microbial Diseases, Osaka University, Osaka, Japan.
Supplemental material for this article may be found at http://jvi.asm.org/.

doi:10.1128/JVI.01115-12

A

Accession No: virus: gene	Bcl-x_L	M11L	DPV84 gp022	SPV12	gp011L	DPV83 gp022	LD17	SPPV14
AAA46628: Myxoma virus: M11L	12.8	***	22.7	24.5	72.6	22.7	22.1	22.1
ABI99009.1: Deerpox virus: DPV84gp022	11.4	22.7	***	28.5	20.8	98.3	31.6	32.2
NP_570172.1: Swinepox virus: SPV12	12.0	24.5	28.5	***	28.2	28.5	31.7	32.3
NP_051900.1: Shope (Rabbit) fibroma virus: gp011L	12.1	72.6	20.8	28.2	***	19.6	21.2	21.2
YP_227399.1: Deerpox virus: DPV83gp022	10.8	22.7	98.3	28.5	19.6	***	31.6	32.2
AAN02583.1: Lumpy skin disease virus: LD17	12.8	22.1	31.6	31.7	21.2	31.6	***	94.4
NP_659590.1: Sheeppox virus: SPPV14	12.2	22.1	32.2	32.3	21.2	32.2	94.4	***

B

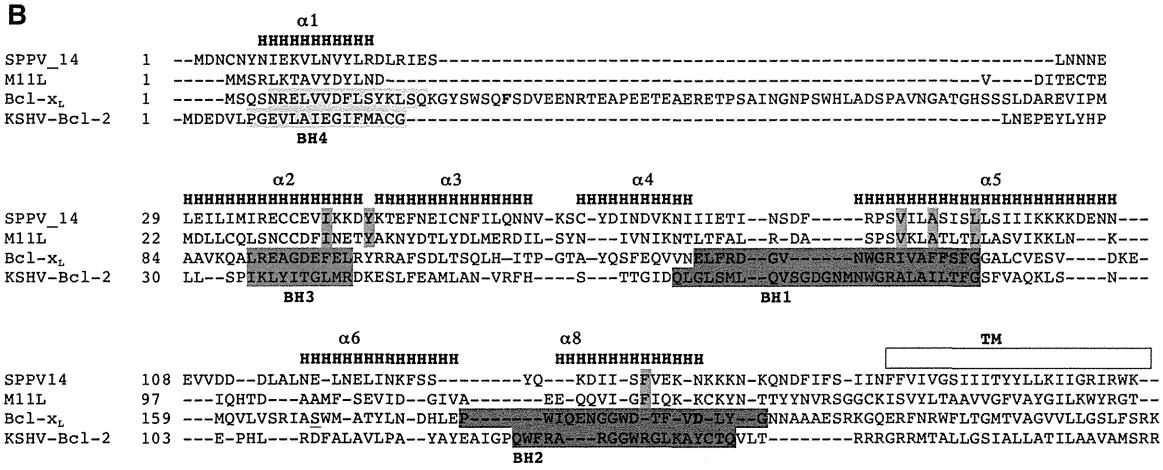

FIG 1 Identifying putative viral Bcl-2 (vBcl-2) homologs. (A) Using myxoma virus M11L as the query sequence in a BLASTP search of the NCBI database, six putative Bcl-2 family proteins encoded by viruses were identified (40). The pairwise identities (percent) in the amino acid sequences between the proteins were determined using ClustalW (57). Note the low sequence homology (<15%) of all the putative vBcl-2 proteins to human Bcl-x_L. (B) The amino acid sequence of a vBcl-2, SPPV14, was structurally aligned with those of myxoma virus M11L (40), mouse Bcl-x_L (44), and KSHV Bcl-2 (35). Based on this alignment, the residues making up α-helices 1 to 8 are marked "H." The colored shading indicates the BH1 (magenta), BH2 (orange), BH3 (green), and BH4 (yellow) Bcl-2 homology regions in Bcl-x_L and KSHV Bcl-2. The residues marked in cyan are those in the BH3 binding groove of M11L and conserved between it and SPPV14 (Fig. 2A). TM indicates the putative transmembrane region as taken from M11L.

Southwest and Central Asia, India, and North Africa and is a significant economic factor due to high mortality rates (50 to 70%), particularly in young animals. In cellular assays, we showed that sheeppox virus SPPV14 potently protects against diverse apoptotic stimuli, and here, we also report studies to define the molecular mechanism of action, and in particular, how it compares with other related proteins, such as myxoma virus M11L. Even though SPPV14 directly inhibits Bax and Bak, similar to M11L, it also binds a unique subset of the BH3-only proteins, suggesting that it may be functionally selected for a specific biological role(s) during the sheeppox virus life cycle.

MATERIALS AND METHODS

Expression and retroviral constructs. The cDNAs of deerpox virus (DPV83gp022 and DPV84gp022), swinepox virus (SPV12), shope fibroma virus (gp011L), lumpy skin disease virus (LD17), and sheeppox virus (SPPV14) were synthesized (GeneScript) and verified by sequencing. All mammalian expression vectors for hemagglutinin (HA)-tagged BH3-only proteins, HA-Bax and HA-Bak, subcloned into pEF PGKhygro have been described previously (9, 34, 46, 67). Similar constructs, made by subcloning into pEF PGKpuro, were generated for all viral proteins. A retroviral expression construct (Bim_S2A) was generated by subcloning into pMIG (murine stem cell virus [*M*SCV]-internal ribosome entry site [*I*RES]-green fluorescent protein [*G*FP], where the GFP sequence is that of enhanced GFP [EGFP]), as previously described (9, 67). The GFP selection cassette was replaced with the hygromycin resistance gene (58) for the constructs expressing viral proteins. Yeast constructs were made by subcloning into the pGALL(TRP) vector, as previously described (22). All cDNAs were of human or viral origin.

Details of all oligonucleotides and constructs used are available on request.

Tissue culture, cell death induction, retroviral infections, and apoptosis assays. All cell lines except Jurkat cells (HEK293T immortalized human embryonal kidney cell line, Phoenix Ecotropic packaging cells [39], and mouse embryonic fibroblasts [MEFs]) were cultured in Dulbecco's modified Eagle's medium (DMEM) supplemented with 10% fetal calf serum (FCS) and in some cases with 250 mM L-asparagine and 50 mM 2-mercaptoethanol. HuTK$^-$-143B and Jurkat cells were obtained from ATCC and maintained as previously described (62). Jurkat cells overexpressing Bcl-2 were generated and cultured as previously described (6); Bak- and Bax-deficient Jurkat cells were a gift from H. Rabinowich (University of Pittsburgh School of Medicine, Pittsburgh, PA) (60).

All MEFs (9, 67) were generated from embryonic day 13 (E13) to E14.5 embryos and immortalized at passages 2 to 4 with simian virus 40 (SV40) large T antigen. All mice used were of C57BL/6 origin or had been backcrossed (>10 generations), and their genotypes were determined as previously described (details are available on request).

Cell death was induced with 10 to 40 μM etoposide, UV irradiation (100 J/m^2), cytosine arabinoside (AraC), ABT-737 (1 μM; Abbott) (47), or FasL (Alexis) or by retroviral infection. pMIG retroviral constructs